The configuration, sensitivity and rapid retreat of the Late Weichselian Icelandic ice sheet.

Henry Patton [a] [*], Alun Hubbard [a,b], Tom Bradwell [c,d], Anders Schomacker [e]

[a] CAGE - Centre for Arctic Gas Hydrate Environment and Climate, Department of Geosciences, UiT The Arctic University of Norway, Tromsø, Norway
[b] Department of Geography and Earth Sciences, Aberystwyth University, Aberystwyth, SY23 3DB, UK
[c] Biological and Environmental Sciences, University of Stirling, FK9 4LA, UK
[d] Department of Geography and Earth Sciences, Aberystwyth University, Aberystwyth, SY23 3DB, UK
[e] Department of Geosciences, UiT The Arctic University of Norway, Tromsø, Norway

* Corresponding author: henry.patton@uit.no

ABSTRACT

The fragmentary glacial-geological record across the Icelandic continental shelf has hampered reconstruction of the volume, extent and chronology of the Late Weichselian ice sheet particularly in key offshore zones. Marine geophysical data collected over the last two decades reveal that the ice sheet likely attained a continental shelf-break position in all sectors during the Last Glacial Maximum, though its precise timing and configuration remains largely unknown. Within this context, we review the available empirical evidence and use a well-constrained three-dimensional thermomechanical model to investigate the drivers of an extensive Late Weichselian Icelandic ice-sheet, its sensitivity to environmental forcing, and phases of deglaciation. Our reconstruction attains the continental shelf break across all sectors with a total ice volume of 5.96 x 10^5 km^3 with high precipitation rates being critical to forcing extensive ice sheet flow offshore. Due to its location astride an active mantle plume, a relatively fast and dynamic ice sheet with a low aspect ratio is maintained. Our results reveal that once initial ice-sheet retreat was triggered through climate warming at 21.8 ka BP, marine deglaciation was rapid and accomplished in all sectors within c. 5 ka at a mean rate of 71 Gt of mass loss per year. This rate of ice wastage is comparable to contemporary rates observed for the West Antarctic ice sheet. The ice sheet subsequently stabilised on shallow pinning points across the near shelf for two millennia, but abrupt atmospheric warming during the Bølling Interstadial forced a second, dramatic collapse of the ice sheet onshore with a net wastage of 221 Gt a^{-1} over 750 years, analogous to contemporary Greenland rates of mass loss. Geothermal conditions impart a significant control on the ice sheet's transient response, particularly during phases of rapid retreat. Insights from this study suggests that large sectors of contemporary ice sheets overlying geothermally active regions, such as Siple Coast, Antarctica, and NE Greenland, have the potential to experience rapid phases of mass loss and deglaciation once initial retreat is initiated.

Keywords: Iceland, Late Weichselian, ice sheet modelling, geothermal, collapse, palaeo reconstruction, shelf edge

1. Introduction

Reconstruction of the Late Weichselian extent and deglaciation history of the Icelandic Ice Sheet (IIS) has largely depended upon a relatively limited and sparsely distributed empirical record, especially in the marine sector (e.g., Norðdahl, 1991; Andrews et al., 2000; Norðdahl et al., 2008; Ingólfsson et al., 2010). Recent geomorphological mapping from shelf-wide acoustic bathymetric surveys has revealed an unprecedented view of the former glacial footprint in all sectors of the Icelandic continental shelf (Spagnolo and Clark, 2009), supporting previous insights from the landform and sediment record for the possibility of an extensive marine-terminating ice sheet at the Last Glacial

48   Maximum (LGM) (Figure 1A) (Ólafsdóttir, 1975; Egloff and Johnson, 1979; Boulton et al., 1988;
49   Syvitski et al., 1999). Previous ice-sheet modelling by Hubbard et al. (2006) revealed that substantial
50   parts of the IIS were potentially marine-based during the LGM. However, equivocal and piecemeal
51   chronological control across the continental shelf has not allowed a full understanding of the form
52   and extent of the LGM ice sheet prior to its retreat into near-shore areas around 16 ka BP (e.g.,
53   Andrews et al., 2000; Jennings et al., 2000; Geirsdóttir et al., 2002; Norðdahl and Pétursson, 2005).
54   From c. 16 ka onwards, radiocarbon dated raised beaches and marine sediments around the present
55   Icelandic coastline, as well as an exceptionally high marine limit of c. 150 m a.s.l. at Stóri-Sandhóll in
56   West Iceland (Ingólfsson and Norðdahl, 2001), indicate that deglaciation onto land occurred
57   extremely rapidly, coinciding with a period of rapid eustatic sea-level rise during the meltwater pulse
58   1A event c. 15.0 ka BP (Ingólfsson and Norðdahl, 2001; Norðdahl and Ingólfsson, 2015).

59   As well as being a largely marine-based ice sheet, the Icelandic domain is of particular interest
60   because of its unique position straddling the tectonically active Mid-Atlantic lithosphere plate
61   boundary (**Figure 1**B). This ~8000 km long spreading centre not only delivers large fluxes of
62   geothermal heat, but is also prone to frequent, large-scale volcanic eruptions (cf. Thordarson and
63   Larsen, 2007). Geothermal heat supply to the subglacial environment can have   a primary influence
64   on ice sheet thermodynamics, through temperature-dependent softening of ice-fabric yielding
65   enhanced basal strain-rates, and/or through elevated levels of melting leading to widespread basal
66   lubrication and motion. During episodes of vigorous subglacial volcanic activity, for example the
67   regular eruptions at Grímsvötn, Bárðarbunga or Kverkfjöll (Óladóttir et al., 2011), the introduction of
68   enhanced basal temperatures exerts a first-order control on ice sheet form, dynamics and stability.
69   During such volcanic episodes, localised rates of subglacial melting exceeds mass-balance terms by
70   an order of magnitude or more, triggering large-scale jökulhlaups (Gudmundsson et al., 1997;
71   Geirsdóttir et al., 1999) promoting fast flow (e.g., Blankenship et al., 1993; Vogel and Tulaczyk,
72   2006).

73   The distribution of geothermal heat flux across Iceland peaks at over 300 mW m^{-2} within the
74   neovolcanic zone, straddling the central rift from SW to NE Iceland (**Figure 1**B). This zone has
75   experienced large variations in magma eruption rates during the last glacial cycle (Jakobsson et al.,
76   1978; Vilmundardóttir and Larsen, 1986; Sigvaldason et al., 1992; Slater et al., 1998), with extrusive
77   episodes 50 times more frequent during deglaciation compared to recent times (Jull and McKenzie,
78   1996; Maclennan et al., 2002). Previous modelling experiments and geophysical data from Iceland
79   indicate that dramatic increases in eruption rates were associated with the onset of deglaciation and
80   glacio-isostatic unloading (Jull and McKenzie, 1996; Slater et al., 1998; Maclennan et al., 2002; Geyer
81   and Bindeman, 2011). However, discriminating the impact of spatial variations in the geothermal
82   flux on the evolution and dynamics of the Icelandic ice-sheet are yet to be fully investigated from a
83   numerical modelling perspective (Bourgeois et al., 2000). This research focus has wide significance
84   given the large sectors of today's Polar ice sheets and smaller ice masses that are located over
85   volcanically active zones characterised by high geothermal fluxes, for example, the Northeast
86   Greenland ice stream (Fahnestock et al., 2001; Rogozhina et al., 2016), the East-West Antarctica
87   boundary (Maule et al., 2005) and the Siple Coast ice streams (Fisher et al., 2015).
88
89   Here we present and examine a new model for the last glaciation of the Icelandic continental shelf
90   within the context of recent chronological and geological insights – particularly in the light of
91   improved shelf-wide geomorphological mapping of the offshore landform record – whilst also
92   reconciling much of the previously published evidence. First, we review the existing empirical
93   evidence that reliably constrains the advance and demise of the last ice sheet, including during the
94   Younger Dryas stadial – a brief cold reversal that interrupted climate amelioration during
95   deglaciation. We then present model output from an optimal experiment, that extends the coupled
96   climate/ice-sheet-flow modelling of Hubbard et al. (2006), putting forward a robust and
97   glaciologically plausible reconstruction of an extensive, marine-based Late Weichselian IIS that

98   reached the continental shelf-edge in all sectors. From this reconstruction we highlight a number of
99   key findings relating to the IIS, including: zonal flow configurations; potential drivers of collapse; as
100   well as its sensitivity and response to a range of internal and external drivers, including the effects of
101   spatially variable geothermal heat flow.

2. The empirical record of glaciation

103   In this section we review the key morphological and chronological evidence for ice-sheet glaciation
104   across the Icelandic continental shelf during the LGM, providing a context in which to place our new
105   modelling results. We assume the LGM of Iceland to have been coeval with the global ice-sheet
106   maximum, which occurred between 26.5-19 ka BP (Peltier and Fairbanks, 2006; Clark et al., 2009).
107   This period is widely referred to as the Late Weichselian glaciation (Europe) (Ingólfsson, 1991;
108   Norðdahl, 1991), equivalent to the Late Wisconsinan of North America, or Late Devensian of the
109   United Kingdom. Offshore, marine geologists commonly use Marine Isotope Stages (MIS) to refer to
110   alternating warm and cold periods – in this case the main Late Weichselian Stadial (and LGM) is
111   associated with MIS2 (29-14 ka BP), proceeding the previous interstadial in MIS3 (60-29 ka BP).

112   Reported ^{14}C ages are recalibrated in this paper to calendar years before present (cal. ka BP) using
113   the program Calib 7.1 (Stuiver and Reimer, 1993) and the IntCal13/MARINE13 calibration curves
114   (Reimer et al., 2013). The marine calibration incorporates a time-dependent global ocean reservoir
115   correction of about 400 years, with a ΔR value of 24±23 used to accommodate local effects
116   (Håkansson, 1983).

2.1. Onset of shelf glaciation (MIS 3/2 transition)

118   Few data constrain the timing or extent of glaciation prior to the LGM, though it is generally
119   assumed the IIS was not on the shelf during the latter part of MIS 3 (Norðdahl and Pétursson, 2005;
120   Andrews, 2008). A till of Mid Weichselian age has been reported from Suðurnes on the Reykjanes
121   peninsula based on two samples dated to c. 31.6 cal. ka BP found within overlying marine sediments
122   (Eiríksson et al., 1997). Based on these dates and sediments, it can be inferred that the southwest
123   coastline was probably ice free during the late Mid Weichselian, tentatively correlated with similar
124   restricted ice-cover in western Norway during the Ålesund interstadial (Figure 1) (Mangerud et al.,
125   1981, 2010). West of Keflavík, till containing fossiliferous sediment clasts overlying striated (215°)
126   bedrock has yielded an age of c. 28.1 cal. ka BP, providing a maximum age for the advance of Late
127   Weichselian ice in this region. However, a weighted mean age from six marine shell samples within
128   stratified sands resting on glacially striated (009°) bedrock north of Rauðamelur suggests that
129   shallow marine conditions may have persisted here until c. 25.8 cal. ka BP (cf. Norðdahl and
130   Pétursson, 2005).

2.2. Last Glacial Maximum (28.1-22.8 cal. ka BP)

2.2.1. The timing of maximum extension

133   For a significant time, constraining the maximum extent of former ice beyond the present-day
134   coastline was limited to observations from islands or low-resolution snapshots of offshore seismic
135   data. Early reports of till, drumlins, roches moutonnées, striae and meltwater channels on the island
136   of Grímsey 40 km off northern Iceland, confirm that ice overrode, and was thick enough to cover the
137   highest parts of the island (> 100 m), at least once (Keith and Jones, 1935; Hoppe, 1968). Although
138   not constrained by any numerical ages, the well preserved meltwater channels and apparent
139   absence of either solifluction cover or of older soils over the thin till deposits, together, were used to
140   suggest a LGM age (Hoppe, 1968).

141   The first description of a submarine glacial landform on the Icelandic continental shelf was reported
142   by Ólafsdóttir (1975), with the discovery of a prominent moraine-like ridge at the western
143   continental shelf break. This feature extends for more than 100 km, lies at water depths of between

200-350 m, and is typically 20 m in relief although in places can reach more than 100 m high (Syvitski
et al., 1999) (**Figure 1**A). A core collected seaward of this Látra Bank end-moraine has provided a
maximum age of this deposit of c. 40.2 ka BP, although dating material was possibly collected from a
pre-LGM erosion surface here (Syvitski et al., 1999). Basal dates from further cores on the adjacent
upper shelf have provided ages of c. 21.4 and 21.6 cal. ka BP, and although do not confirm or refute
the presence of LGM ice at the moraine, imply only modest sediment accumulation rates were
achieved in this sector (10.2 cm kyr^{-1}) (Andrews et al., 2000). Compared with an upper shelf slope
core taken from the opposite side of the Denmark Strait, below the mouth of Kangerlussuaq Trough,
the accumulation rates in the Icelandic sector are three times lower (30.6 cm kyr^{-1}) (Andrews et al.,
1998). Andrews et al. (2000) therefore suggested that the western Icelandic ice sheet margin was
either not a major contributor of sediment to the upper slope, or that the area was by-passed by
various downslope transport processes during the LGM (e.g., Syvitski et al., 1999).

Further geophysical surveying offshore has revealed major till deposits up to 100 m thick at the
continental shelf edge in the south-eastern sector, as well as an associated retreat moraine complex
– the Tvísker moraine – 20 km from the present coastline (Boulton et al., 1988). Off southwestern
Iceland, Egloff and Johnson (1979) also found an acoustically transparent, 100-350 m thick upper
layer present adjacent to the shelf edge. With no chronological control, this sediment package,
resting on a probable erosional surface, was interpreted to represent morainic deposits of Late
Pleistocene age.

More recent, systematic coring efforts north and northwest of Iceland have attempted to pinpoint
the LGM ice sheet extent on the continental shelf, though results proved largely equivocal. Three
cores recovered from within Reykjafjarðaráll, a large trough extending from north Iceland towards
the shelf break, revealed a broad cover of matrix-supported diamicton overlain by fine-grained
postglacial muds (Andrews and Helgadóttir, 2003). All foraminifera samples within the lower
diamicton provided consistently old dates (27-44 cal. ka BP), while radiocarbon dates immediately
above the diamicton yielded ages of c. 13 cal. ka BP. The preferred interpretation by these authors
was that the stratigraphy and chronology could be best explained by Late Weichselian ice
overrunning the sites, reworking glacio-marine sediments deposited >25 cal. ka BP, and persisting in
the trough until c. 13 cal. ka BP (Andrews and Helgadóttir, 2003; Principato et al., 2005). Based on
this conclusion, the core locations thus represent a minimum spatial constraint of the maximum Late
Weichselian ice-sheet margin.

An alternative interpretation for the "old" (> 25 cal. ka BP) lower diamicton is that it represents *in
situ* glacio-marine sediments that did not directly interact with an ice sheet, thus delimiting the
maximum spatial extent of the LGM ice sheet. Despite an absence of geomorphological evidence,
such as end-moraines or grounding-zone features within Reykjafjarðaráll to support a "restricted"
LGM ice sheet in this sector (Andrews and Helgadóttir, 2003; Spagnolo and Clark, 2009), this view
has generally persisted within the literature and has formed maximal constraints for a number of
conceptual and numerical reconstructions (Andrews et al., 2000; Norðdahl and Pétursson, 2005;
Hubbard et al., 2006; Norðdahl and Ingólfsson, 2015).

Djúpáll, a narrow cross-shelf extending northwest from Vestfirðir is traversed by a number of
prominent moraines, mapped from seismic profiles (Andrews et al., 2002); and seen on singlebeam
(Olex) bathymetric data (Spagnolo and Clark, 2009). Two anomalously "old" (> 35 cal. ka BP) dates
from foraminifera found within a massive diamict underlying laminated marine deposits have been
similarly used to infer a restricted LGM ice sheet on the NW shelf (Andrews et al., 2002b; Geirsdóttir
et al., 2002). However, more recent data has cast doubt on this interpretation, based on the
probability that the dated foraminifera from the underlying diamict here are also reworked
(Quillmann et al., 2009). Taking this into account, one corrected radiocarbon date of 22.8 cal. ka BP
from massive to faintly laminated glacimarine sediments (in core B997-338PC) provides a useful

192 minimum constraint for the retreat of the LGM ice sheet in this sector (Andrews et al., 2002b;
193 Geirsdóttir et al., 2002). Further basal core dates in the same part of the trough imply an average
194 sediment accumulation rate of around 30 cm kyr^{-1} during deglaciation (Andrews et al., 2000).

195 From an overview of the existing radiocarbon chronology offshore, it is clear that dating control on
196 the maximum extent of the LGM ice sheet is loose and spatially incoherent (Figure 1). Despite a
197 number of ages being affected by glacial reworking of the sediments, two dated cores from the
198 western sector of the ice sheet constrain a maximum and minimum age for the timing of ice advance
199 and retreat, indicating that Late Weichselian peak ice extent was probably attained sometime
200 between 25.8 and 22.8 cal. ka BP (Andrews et al., 2002b; Geirsdóttir et al., 2002).

2.2.2. Shelf-edge glaciation?
202 A significant advance in our understanding of the offshore glacial footprint came with the release of
203 a bathymetric database compiled, processed and managed by Olex AS. The Olex bathymetric
204 database and resulting imagery is based upon single-beam echo-sounding, mostly derived from
205 fishing vessels, with a vertical resolution of ±1 m in water depths > 100 m, and 0.1 m at depths < 100
206 m. The horizontal positional error is limited by the precision of non-corrected, on-board Global
207 Positioning Systems, but is generally ~10 m and is further reduced by the cross-correlation of
208 multiple, coincident soundings. Mapping from this dataset allowed an unprecedented synoptic view
209 of glacial landforms on c. 80% of the continental shelf around Iceland. From this dataset, Spagnolo &
210 Clark (2009) mapped several hundred newly identified landforms, including submarine end moraines
211 and streamlined bedforms, which comprise the broad-scale glacial footprint of IIS extent and
212 subsequent retreat.

213 The recent release of the EMODnet Digital Terrain Model – a composite bathymetric dataset, with
214 data gaps filled using the GEBCO 2014 30” dataset to a horizontal resolution of 7.5 arc seconds
215 (http://www.emodnet-hydrography.eu/) – has since provided complete bathymetric coverage of the
216 Icelandic continental shelf at a resolution suitable for mapping large glacial landforms. Here, we
217 consolidate and extend previous mapping offshore (Ólafsdóttir, 1975; Boulton et al., 1988; Spagnolo
218 and Clark, 2009) with prominent features observed from Landsat imagery onshore as well as new
219 landforms observed from previous data gaps offshore (**Figure 2**). The geomorphological
220 interpretations made here are guided by the context of previous work described above.

221 The largest and most prominent geomorphological features on the continental shelf are a radial
222 system of overdeepened cross-shelf troughs that extend from major onshore valley systems and
223 widen towards the continental shelf edge. Compared to other cross-shelf troughs in high-latitude
224 settings, such as around Greenland, Norway and northeast Canada, they are relatively shallow, and
225 are draped with a thin layer of deglacial sediments, indicative of moderate rates of glacial erosion
226 (Syvitski et al., 1987; Andrews et al., 2000). Most Icelandic cross-shelf troughs terminate with a
227 reverse slope in long-profile and a bulging, arcuate terminus in planform (**Figure 2**C). Their
228 association with distinct sets of large submarine streamlined ridges, running parallel to trough axes,
229 as well as similar streamlined mega-lineations and striae onshore (Norðdahl, 1991; Bourgeois et al.,
230 2000; Principato et al., 2016), strongly suggest that these areas were regions of streaming ice flow,
231 indicative of widespread temperate subglacial conditions. Often associated with these offshore
232 mega-lineations, are parallel channels up to 75 m in depth, 3 km wide and 20 km long, found incising
233 to depths of 360 m below present-day sea level. Based on their morphological affinity with glacial
234 channels elsewhere, and their location within zones of former temperate-based ice, these features
235 are likely to have formed by meltwater erosion during repeated episodes of grounded ice-sheet
236 advance (e.g. Ó Cofaigh, 1996).

238 Broad and well-defined features interpreted as moraines are located near the Icelandic shelf edge in
239 most sectors (**Figure 2Figure 2**), of which two features have been previously identified though not

240 radiocarbon dated directly (Ólafsdóttir, 1975; Boulton et al., 1988; Syvitski et al., 1999) (Figure 1).
241 Moraine ridge lengths range from 6 to ~80 km, and their arcuate form is typical of end moraines
242 formed at grounded terrestrial ice-sheet margins. However, it cannot be completely discounted that
243 some of the ridges could represent subaqueous morainal banks – the product of grounded, quasi-
244 stable, water-terminating glaciers. A large ridge running parallel to the trough axis north of
245 Tröllaskagi is interpreted to be a medial-type moraine, formed at the junction of converging ice flow
246 units and downglacier of a topographic high.
247
248 Included in this landform group are a set of prominent ridges to the north of Vestfirðir (**Figure 2**B),
249 not previously described before in the literature due to bathymetry data gaps. Although the timing
250 of glaciation is still poorly constrained, their position adjacent to the shelf edge (consistent with
251 other sectors of the continental shelf), the northerly continuation of mapped MSGLs in nearby
252 troughs, the presence of perennial-sea ice cover stabilising calving margins around Iceland during
253 stadial conditions (Hoff et al., 2016), and the presence of subglacially reworked glacial diamicton in
254 present-day water depths of at least 347 m (Andrews et al., 2000) all indicate that grounded ice
255 during the Late Weichselian was probably more extensive in this sector than has been previously
256 speculated (Andrews et al., 2000; Norðdahl and Pétursson, 2005; Hubbard et al., 2006; Norðdahl and
257 Ingólfsson, 2015).Additional sets of arcuate moraines are present closer to the present day Vestfirðir
258 shoreline, demarcating potential still-stands or re-advances of the ice-sheet margin during
259 deglaciation (**Figure 2**) (Andrews et al., 2002b). Many of these moraines are associated with
260 extensive iceberg keel scouring mapped to depths of 180 m below present sea-level (Syvitski et al.,
261 1999).
262
263 Despite a widespread coverage of glacial landforms across the continental shelf, limited marine
264 coring combined with significant reworking of sediments during the last glacial cycle offshore (e.g
265 Syvitski et al., 1999; Andrews et al., 2000; Andrews and Helgadóttir, 2003; Principato et al., 2005)
266 means that robust chronological constraints on the extension of the LGM ice sheet are,
267 unfortunately, lacking. Notwithstanding this poor chronological control, the geomorphological
268 footprint of shelf-edge glaciation in all sectors, including newly identified moraine ridges north of
269 Vestfirðir (**Figure 2**C), leaves extensive ice cover in all sectors as the most probable and compelling
270 scenario for Late Weichselian glaciation over Iceland.
271
272 Further support for an extensive shelf-edge IIS configuration comes from the maximal extents of
273 neighbouring mid-to-high-latitude ice sheets in the North Atlantic region at LGM. The most recent
274 compilation of dates and reconstructions of the Eurasian Ice Sheet (Hughes et al., 2016) places the
275 "most credible" ice sheet limits at, or close to, the continental shelf break at LGM (c. 27 ka) in the
276 British/North Sea, Norwegian and Svalbard/Barents Sea sectors. Although dating control in these
277 marine sectors is still not particularly firm, the compelling convergence of several lines of evidence
278 (i.e. submarine geomorphology, seismic stratigraphy, seabed cores, ice-rafted debris records, and
279 key dates) (cf. Ottesen et al., 2002; Clark et al., 2012; Patton et al., 2015) with updated numerical
280 modelling (e.g., Hubbard et al., 2009; Patton et al., 2016) strongly suggest a shelf-edge scenario for
281 the Eurasian ice-sheet complex at the LGM. Across the Denmark Strait, the southeastern sector (60-
282 68°N) of the Greenland Ice Sheet also extended to the continental shelf edge at its Late Weichselian
283 maximum (Roberts et al., 2008; Dowdeswell et al., 2010; Vasskog et al., 2015), with major ice
284 streams supplying sediment to trough-mouth fans on the continental slope. Even the small and
285 dynamic ice cap on the Faroe Islands is believed to have fed shelf-edge depocentres at maximum
286 extent during the LGM (Nielsen et al., 2007).

287 ### 2.2.3. Ice thickness
288 Onshore in Iceland, table mountains, erosional trimlines and glacial striae have all been used to
289 reconstruct overall ice sheet thickness (Walker, 1965; Einarsson, 1968; Hjort et al., 1985; Norðdahl,
290 1991; Van Vliet-Lanoë et al., 2007). An extensive suite of cosmogenic ^{3}He exposure ages derived

from table mountain summits within the neovolcanic zone provide an excellent constraint for ice-thickness changes during deglaciation (Licciardi et al., 2007). Moreover, if the exposure ages correctly date the timing of deglacial eruptions, the table mountain elevations also provide minimum altitudes for the LGM ice surface. These range from Herðubreið (1682 m a.s.l.) beneath the probable central ice divide, to Hafrafell (512 m a.s.l.) at the present-day northeast coastline (Licciardi et al., 2007).

The Tröllaskagi highlands have historically been the focus of numerous attempts to delimit ice-sheet thickness at the LGM. Based on geomorphological features such as lateral moraines, meltwater channels, upper limits of glacial erosion, and differences in weathering, a concept for maximum Weichselian glaciation in North Iceland was proposed that included significant ice-free areas interspersed by low gradient and interconnected ice streams (Norðdahl, 1991). Furthermore, the dendritic nature of the Tröllaskagi valley system was cited as evidence for glaciation by independent local ice domes rather than invasion from an inland ice sheet (Norðdahl, 1991). The existence of purported unglaciated coastal mountain areas, such as in the Tröllaskagi highlands, has also been cited as evidence in support of possible refugia sites for hardy plant species through the Weichselian – helping to explain the relatively high Holocene species diversity (e.g., Rundgren and Ingólfsson, 1999).

It is worth noting that previous model experiments, where the extent of Late Weichselian ice is limited at Grímsey, can reproduce ice-free areas across the Tröllaskagi highlands. However, modelled ice thicknesses vary significantly, by up to +63%, with perturbations in input parameters, boundary conditions and modelled extent (Hubbard et al., 2006). Studies from around Europe have shown that distinguishing between zones that were completely ice-free and those protected by cold based/non-erosive ice based on geomorphology alone is a complex task, with ice-sheet thicknesses often underestimated (Fabel et al., 2002; Ballantyne, 2010). Unfortunately, the predominantly basaltic bedrock of Iceland precludes the collection of common paired cosmogenic isotopes (e.g., ^{10}Be and ^{26}Al) for determining complex exposure histories from mountain summits.

Deglacial cosmogenic ^{36}Cl exposure ages from erratic boulders in Vestfirðir are spread across the interval from 26 to 15 ka BP, indicating that the LGM ice sheet could have reached its maximum prior to this time; subsumed summits to at least 650 m a.s.l., and probably extended a considerable distance beyond the present-day coastline around northwest Iceland (Brynjólfsson et al., 2015). Brynjólfsson et al. (2015) interpreted the presence of erratic boulders sitting on top of an undisturbed block field as evidence of cold-based LGM ice over the uplands of Vestfirðir. Their conceptual model indicates warm-based ice in the lowlands as witnessed by the fjords, glacially eroded valleys, and widespread evidence of subglacial erosion.

2.3. Deglaciation (<22.8 cal. ka BP)
Dated glacimarine sediments in cores from Djúpáll reveal deglaciation was underway on the outer shelfby 22.8 cal. ka BP and had retreated to the mid shelf before 18.5 cal. ka BP (Andrews et al., 2000, 2002b). Furthermore, a basal date from marine sediments in a core north of Grímsey indicates that Atlantic Waters were present on the northern shelf >16.5 cal. ka BP (Eiríksson et al., 2000).

Onshore, cosmogenic exposure ages from glacially eroded bedrock in northern Vestfirðir strongly suggest that thinning of the ice sheet was underway soon after the LGM. Two samples collected from bedrock on Ármúli (Ísafjarðardjúp - 370 m a.s.l.) have produced an average ^{36}Cl age of 22.3 ka (20.4 ka with atmospheric correction) (Principato et al., 2006), whilst exposure ages from high-elevation erratic boulders on Leirufjall suggest ice-sheet thinning over Vestfirðir started as early as c. 26 cal. ka BP (Brynjólfsson et al., 2015). The ages of Principato et al. (2006) and Brynjólfsson et al. (2015) are, however, not directly comparable because of the different production rates and scaling parameters used in these respective studies.

2.3.1. Bølling - Allerød (15.4 – 13.0 cal. ka BP)

Seismic profiling and sediment core studies indicate that deglaciation of the Icelandic continental shelf between c. 15-13 cal. ka BP occurred rapidly (Syvitski et al., 1999; Jennings et al., 2000; Andrews and Helgadóttir, 2003; Andrews, 2005), coeval with the northward migration of the Polar Front as well as rapidly rising eustatic sea-levels during the Bølling interstadial (Ingólfsson et al., 1997; Eiríksson et al., 2000; Ingólfsson and Norðdahl, 2001; Lambeck et al., 2014). Over the course of a few centuries between c. 14.7-14.3 cal. ka BP global sea-levels underwent a period of massive change, rising on average at a rate greater than 40 mm per year (Deschamps et al., 2012). Referred to as meltwater pulse 1A, this event was probably a significant driver for the destabilisation of marine-terminating glaciers around Iceland (Norðdahl and Ingólfsson, 2015).

Geological evidence for rapid retreat at this time in part comes from the relatively thin drape of deglacial marine sediments over the continental shelf (Principato et al., 2005; Andrews, 2007; Geirsdóttir et al., 2007), but is also supported by a number of key chronological constraints. Dates from the near base of glacimarine sediments in Jökuldjúp (15.1-14.9 cal. ka BP; Jennings et al., 2000; Principato et al., 2005) and in northward flowing troughs of Húnaflóadjúp (16.1-15.6 cal. ka BP; Andrews and Helgadóttir, 2003; Principato et al., 2005) indicate ice-free conditions offshore by this time (**Figure 1**B). Similarly aged radiocarbon dates in western Iceland, usually associated with high raised marine shorelines (105-150 m a.s.l.), provide strong evidence that coastal areas here were deglaciated and still submerged between c. 15.0-14.7 cal. ka BP (Ashwell, 1975; Geirsdóttir and Eiriksson, 1994; Ingólfsson and Norðdahl, 2001; Norðdahl and Pétursson, 2005; Norðdahl and Ingólfsson, 2015), also indicating a potentially catastrophic collapse of the near-shelf sectors of Jökuldjúp. A further onshore date of 14.9 cal. ka BP constrains a Bølling marine transgression c. 60 m a.s.l. in northeast Iceland (Norðdahl and Pétursson, 2005), with additional Bølling-aged raised marine shorelines reported on the Reykjanes peninsula (70 m a.s.l.), Breiðafjörður (90-110 m a.s.l.), Vestfirðir (75-95 m a.s.l.), and the Skagi peninsula (65 m a.s.l.) (cf. Norðdahl and Pétursson, 2005). Given the generally low viscosity of the Iceland lithosphere and asthenosphere, it has been additionally argued that the very high elevations of these raised shorelines could only have formed under extremely rapid deglaciation (Ingólfsson and Norðdahl, 2001).

More quantitative support for this observation has come recently from cosmogenic-nuclide exposure-age dating of table mountain summits within the Iceland neovolcanic zone . The premise that a pulse of enhanced volcanic production immediately followed deglaciation has existed for some time, although the timing and mechanistic link is not well constrained (Jakobsson et al., 1978; Vilmundardóttir and Larsen, 1986; Sigvaldason et al., 1992; Slater et al., 1998; Maclennan et al., 2002; Sinton et al., 2005). However, the mean ages of 42 individual cosmogenic-exposure ages from 13 different table mountains within the neovolcanic zone reveal two discrete intervals of active table mountain growth at c. 14.4-14.2 ka and 11.1-10.5 ka, suggesting that these periods were associated with episodes of rapid ice-sheet thinning or unloading that stimulated enhanced volcanic activity (Licciardi et al., 2007).

Towards the end of the Bølling-Allerød Interstadial and onset of the Younger Dryas Stadial, the IIS began to expand once more. This period is marked by rising relative sea levels and general cooling of the marine environment – witnessed by the appearance of High Arctic mollusc species in western Iceland (Norðdahl and Pétursson, 2005). Rapid isostatic uplift of the crust in response to the swift collapse of marine-based ice-sheet sectors (e.g., Sigmundsson, 1991; Ingólfsson et al., 1995) may also have contributed to a regional relative lowering of the equilibrium-line altitude of the ice sheet, thus enhancing snow accumulation, ice sheet growth and glacier advance.

2.3.2. Younger Dryas & Early Holocene (13.0-10.0 cal. ka BP)

Truncated raised shorelines in the mouths of fjords and valleys around Iceland demonstrate that the ice sheet expanded during the Younger Dryas across many coastal sites that had been ice-free since

386   Bølling deglaciation (Norðdahl and Pétursson, 2005; cf. Ingólfsson et al., 2010). In northern Iceland
387   the ice sheet extended offshore into various fjords during the Younger Dryas, although elsewhere it
388   was generally less extensive than the present-day coastline (Norðdahl and Haflidason, 1992;
389   Geirsdóttir et al., 2000; Principato et al., 2006; Brynjólfsson et al., 2015) (**Figure 1**). Truncated
390   shorelines of probable Younger Dryas age suggest that the tip of the Langanes Peninsula remained
391   ice free during this stadial, with the glacier margin some 5 km inland from the present coast
392   (Norðdahl and Hjort, 1995). Marine shorelines of an assumed Younger Dryas age between 58 and 35
393   m a.s.l. in eastern Iceland also suggest ice was grounded in the heads of the eastern fjords, with
394   many promontories and headlands remaining ice-free (Norðdahl and Einarsson, 2001).

395   A prominent example of interrupted retreat of the IIS during the Lateglacial period is the Búði
396   moraine system in south-central Iceland – a composite feature of multiple, discontinuous ridges.
397   Most of this complex shows deltaic characteristics with distinct foreset bedding and glaciofluvial
398   sandur accumulation, indicating a transition between marine-coastal and terrestrial environments
399   and demonstrating that the southern lowlands of Iceland were submerged at the time of deposition
400   (Hjartarson and Ingólfsson, 1988; Geirsdóttir et al., 1997, 2000). The occurrence of 11.98 ka BP
401   Vedde Ash in forefield lake sediments, an extensive tephra marker layer associated with the
402   pyroclastic eruption of Katla (Grönvold et al., 1995), along with *in situ* radiocarbon dates (Table 1)
403   support a Younger Dryas age for the Outer Búði moraine c. 12.1-11.9 ka BP (Geirsdóttir et al., 1997;
404   Norðdahl and Pétursson, 2005; Geirsdóttir, 2011). In central Iceland, cosmogenic exposure ages
405   from table mountains reveal inland ice thickness at this time was c. 550 m (Licciardi et al., 2007).

406   Offshore ice-rafted debris records from cores within Ísafjarðardjúp reveal that calving glaciers were
407   present on Vestfirðir from the Younger Dryas through to the earliest Holocene – known as the
408   Preboreal (ca. 11 ka BP), with submerged moraines in fjords appearing to support stepwise retreat
409   of this margin (Geirsdóttir et al., 2002). More recent exposure-age dating appears to show that
410   glacier retreat was asynchronous between various northwest fjords between the Allerød and
411   Holocene, with time lags of up to 2-5 ka (Principato et al., 2006; Brynjólfsson et al., 2015). The
412   abrupt climatic termination of the Younger Dryas Stadial (Dansgaard et al., 1989) prompted
413   widespread retreat of the residual IIS, inducing rapid glacio-isostatic rebound (Norðdahl and
414   Einarsson, 2001) that triggered a short-lived volcanic eruptive phase (Licciardi et al., 2007) as well as
415   falling relative sea-levels.

416   The last, short-lived, advance of the IIS occurred during climate deterioration within the earliest
417   Holocene or Preboreal (c. 11.2 cal. ka BP) (Rundgren et al., 1997; Norðdahl and Einarsson, 2001). Like
418   the Younger Dryas, reconstruction of the ice extent at this time comes largely from the distribution
419   of raised shorelines and ice-marginal landforms, and tephrochronological correlations, associated
420   with a 20-25 m RSL transgression (Ingólfsson et al., 1995, 2010; Norðdahl and Pétursson, 2005). The
421   first island-wide palaeoglaciological reconstruction by Norðdahl and Pétursson (2005) of this time
422   interval reveals an ice sheet only c. 20% smaller than the Younger Dryas ice sheet and with a similar
423   configuration. For example, the Inner Búði moraine system was formed during a Preboreal advance
424   from 11.5-10.1 ka BP, with dated marine molluscs found both in front of and behind the moraine
425   complex (Hjartarson and Ingólfsson, 1988; Geirsdóttir et al., 1997; Norðdahl and Pétursson, 2005).
426   The greatest differences though lie in the major outlet glaciers of northern Iceland, which had
427   retreated some 30-50 km from the mapped Younger Dryas limits.

428   By 10.3 ka BP, the main ice sheet had all but disappeared across the Icelandic highlands. This is
429   confirmed by the presence of the Saksunarvatn tephra (c. 10.2 ka, Grönvold et al., 1995; Andrews et
430   al., 2002a) in a number of high-elevation sites, including glacial lake Hvítárvatn (Stötter et al., 1999;
431   Caseldine et al., 2003; Geirsdóttir et al., 2009; Larsen et al., 2012).

3. The ice flow model

Here we use a 3D, time-integrated ice sheet model based on the conservation of mass and heat utilizing Glen's (1955) flow law implemented under a first-order approximation of the Stokes-equations adopted from Blatter (1995), Hubbard (1999, 2000), Marshall et al. (2005), and Pollard and DeConto (2007). It has previously been applied to Iceland (Hubbard, 2006; Hubbard et al., 2006), the British Isles (Golledge et al., 2008; Hubbard et al., 2009; Patton et al., 2013), Patagonia (Hubbard et al., 2005) and the Eurasian ice-sheet complex (Patton et al., 2016) to investigate the build-up, extent and deglaciation of the palaeo-ice sheets that occupied these regions. The approach to solving the membrane stress and associated strain fields equate to the L1L2 classification of higher-order models defined by Hindmarsh (2004) that includes longitudinal deviatoric stresses that act to stabilise ice flow over steep relief with high rates of basal lubrication and motion. The model is thermomechanically coupled and temperature-dependent internal flow (ice deformation) is complimented by basal motion calculated using Weertman's (1964) sliding relation when subglacial temperatures attain pressure melting point. The model performs well when compared with second-order and full-Stokes schemes in the ISMIP-HOM benchmark experiments (Pattyn et al., 2008) and has been applied and validated against surface and englacial velocity measurements at Haut Glacier d'Arolla (Hubbard et al., 1998) and Glacier de Tsanfleuron (Hubbard et al., 2003; Chandler et al., 2006) under variable ice rheology. Model derivation, assumptions, limitations and implementation are found in the references above and description here is limited to specific implementation for Iceland.

The model requires key input data and boundary conditions: (i) the present-day reference climate comprising monthly mean air temperature (MMAT) and precipitation, (ii) relaxed basal topography, and (iii) the geothermal heat flux. The model is integrated forward through time from an initial (ice-free) condition and is forced through a time-series of temperature, precipitation and eustatic sea-level perturbations. Key parameters, constants and values are presented in Table 2.

3.1. Climate and mass balance

Surface mass balance, which accounts for ice gains and losses from the ice-sheet surface, is determined by a positive degree-day (PDD) scheme, applied according to Laumann and Reeh (1993), and derives total melt from integrated monthly positive temperatures. Monthly temperature is calculated from the MMAT, perturbed by a sinusoidal function whose maximum and minimum amplitudes are determined by mean monthly July and January temperatures, respectively. Daily cumulative PDDs for each month are calculated using a probability function based on a relationship between the standard deviation of daily to mean monthly temperature. Palaeo-climate forcing is implemented from the 50-year interval NGRIP δ^{18}O record (Andersen et al., 2004), scaled between a maximum prescribed temperature depression and present-day conditions. The inclusion of an additional bulk offset within the temperature scaling calculation controls the degree of fluctuation within the forcing record. Precipitation distributed evenly throughout the year, and accumulates as snow when the surface temperature falls below a threshold of 1 °C. Winter expansion of sea ice across the North Atlantic probably impacted upon precipitation seasonality during stadial conditions, leading to a summer bias in the annual precipitation distribution across maritime sectors (Thomas et al., 2008; Koenigk et al., 2009). Annual precipitation totals were thus likely greater than implied by the effective precipitation volumes recorded by glacier geometries due to the expected increased losses from the system associated with summer rainfall (Golledge et al., 2010).

Both temperature and precipitation adjust to the evolving ice-sheet surface (corrected for isostatic loading) through applied lapse rates, derived from multiple-regression analyses of meteorological observations over the reference period (1961-1990 provided by the Icelandic Meteorological Office) (Björnsson et al., 2007; Crochet et al., 2007) (**Figure 3**A-C).

479   Independent variables used in the regression analysis for temperature include easting, northing, and
480   elevation. To determine the spatial pattern of the precipitation, an additional independent
481   parameter was used - δ_{temp} - the residual difference between the summer and winter temperatures,
482   which provides a convenient proxy for "continentality". R^2 values of 90 % and 88 % give confidence
483   that these three variables robustly account for the main temperature variability across the model
484   domain. The R^2 for the present-day distribution of annual precipitation indicates a weaker
485   correlation at c. 62% (Table S1). A limitation of the model is that we do not calculate the general
486   circulation. Large-scale changes in climate related to shifts in atmospheric circulation are thus not
487   accounted for, although broad scale distributions, for example rain shadow effects, can be
488   incorporated manually by the application of linear gradients.

489   Mass wastage at tidewater margins is calculated according to the frontal calving geometry using an
490   empirically derived depth-related algorithm (Brown et al., 1982). This calving parameterisation is
491   not physically based but does, implicitly, account for the area of the tidewater front exposed to
492   submarine melting – an important, significant yet under-represented component of mass loss from
493   the termini and ice shelves of marine-ice sheets (e.g. Rignot et al., 2010; Nick et al., 2012; Chauché
494   et al., 2014).

3.2. Topography
496   The model is applied to a finite-difference domain of 1300 x 650 km at 2000 m horizontal resolution
497   encompassing the entire Icelandic continental shelf. Present-day onshore topography was extracted
498   from digital elevation data sourced from http://www.viewfinderpanoramas.org/dem3.html with a
499   resolution of 3 arc seconds (c. 90 m), and offshore bathymetry from the GEBCO_08 world data set at
500   a resolution of 30 arc seconds. All topographic data were merged onto a Gall cylindrical equal-area
501   projection, and a point grid used to extract the required elevation data in order of priority (**Figure
502   3**D).

3.3. Geothermal heat flux
504   Subsurface thermal gradients are dependent on four factors: 1) the regional heat flow through the
505   crust, 2) hydrothermal activity, 3) permeability of the rock, and, 4) the residual heat build-up in
506   extinct volcanic centres (Flóvenz and Sæmundsson, 1993). Given the strong influence of the active
507   volcanic rift zone dissecting Iceland, background heat-flux values vary considerably from 80 to 310
508   mW m^{-2} across the domain. The pattern of geothermal heat flux used as a basal thermal boundary
509   condition was determined from temperature measurements taken at the base of shallow (30-60 m)
510   boreholes (Flóvenz and Sæmundsson, 1993) that are interpolated across the model domain using a
511   standard kriging gridding algorithm with a linear variogram model containing no anisotropic
512   weighting (**Figure 3**E).

4. Experiment results and selection

515   Although the model has a limited number of primary parameters (cf. Table 1), the uncertainty in
516   model trajectory can be significantly reduced through sensible – empirically guided – parameter
517   choices, and critical comparison of output with geological evidence. However, the challenge in
518   accurately reconstructing the IIS is further compounded by the fact that extreme rates of mass-loss
519   are possible across the marine-terminating margins through calving and submarine melting,
520   introducing potential non-linear feedbacks within the climate–ice-sheet–ocean system. Onshore, the
521   experimental problem is better defined, as here the first-order control on terrestrial ice masses is
522   the spatial distribution of accumulation and ablation (cf. Hindmarsh, 1993). Hence, once offshore,
523   marine ice-sheet dynamics add a level of system complexity regardless of climate forcing. Given the
524   poor chronological constraints available for determining rates of ice-sheet advance and retreat
525   (section 2), any reconstruction generated will remain symptomatically ambiguous.

526 Despite such uncertainties, broad thresholds for imposed climatic forcing can be identified through
527 incremental iteration of the principal parameters. Furthermore, the optimal reference experiment
528 singled out in this study constitutes a result considered to best represent and honour the most
529 recent advances in our understanding of the extent and dynamics of the former ice sheet. Despite
530 the disparate chronological and geomorphological constraints previously described (cf. section 2)
531 (**Figure 1-2**), the reconstruction is glaciologically consistent and provides a basis for future
532 refinement once further empirical constraints emerge. Key time-slices tracking the evolution of ice
533 sheet extent and its associated flow dynamics are provided (**Figure 4**), with corresponding time-
534 series of volume and area (**Figure 5**).

4.1. Reference experiment

536 A number of broad features within the reference experiment derived here are consistent with
537 previous empirical and modelled IIS reconstructions: i) the broadly trending east-west orientated
538 ice-divide centred over the northern margin of present-day Vatnajökull and its major dog-leg
539 extension into Vestfirðir, ii) efficient drainage via numerous topographically constrained outlet
540 glaciers that penetrate far into the interior of the ice sheet via the major fjord systems, and iii) a
541 grounding-line well below LGM sea-level driving high rates of calving in marine-sectors.

542 The reference experiment requires a mean annual air temperature (MAAT) depression of at least
543 9.5°C from present day values over the duration of the LGM. Additional cooling beyond this
544 threshold has little impact on the ice sheet reaching its maximum extent at the shelf edge, with
545 precipitation rates becoming the key climatic variable for determining the pace of ice build-up and
546 total volume.

547 However, there are numerous and significant differences between the reference experiment
548 presented here and that of Hubbard et al. (2006) most notably in terms of ice sheet advance and
549 extent to the continental shelf edge. Whereas the reconstruction of Hubbard (2006) actively limited
550 ice development on the Langanes Peninsula and the northern shelf through the imposition of strong
551 precipitation gradients, here ice expansion to the north, east and west of Iceland is unhampered
552 (**Figure 4**). Precipitation rates in our reference experiment are reduced across the whole domain
553 during the LGM by 40%, with a positive west to east gradient of 35 % imposed from 17.53°W.
554 Moreover, whereas Hubbard (2006) initiates the LGM experiments at 24 ka BP with a 5°C cooling
555 and terminates them at 21 ka BP; experiments here are initiated at 35 ka BP and are forward
556 integrated until 10 ka BP. The increased model time-span enables the ice-sheet to initiate and its
557 climate and flow dynamics to physically and numerically stabilise and relax completely to the
558 imposed forcing.

559 The ice sheet's relatively simple form and large, central ice divide mean that growth and retreat of
560 the ice sheet is largely radially symmetrical across marine sectors. Exceptions are along the southern
561 coast where the narrow width of the continental shelf acts as a natural topographic barrier to ice
562 sheet growth. Ice flow is relatively stable throughout the maximum configuration with large sectors
563 of the ice sheet bed consistently at pressure-melting point (**Figure 6**A), resulting in stable patterns of
564 basal motion and fast-flow drainage throughout. The absence of strong ice-stream switching
565 throughout this maximal configuration, as has been suggested for other palaeo ice sheets
566 (MacAyeal, 1993; cf. Hubbard et al., 2009; Stokes et al., 2016), yields stable margins offshore for
567 almost 2,000 yr during the LGM (**Figure 7**).

568 The modelled LGM ice sheet has a maximum total area of 5.62×10^5 km^2 and a concomitant volume
569 of 6.58×10^5 km^3 - a two-fold increase on both metrics compared to the reconstruction by Hubbard
570 et al. (2006) - and equates to a net eustatic contribution of c. 1.53 m of global sea-level equivalent.
571 For ice grounded below sea-level, the net mass contribution to sea-level rise was taken from ice
572 lying between the flotation level and the ice surface, calculated assuming an ice density of 917 kg m^{-3}
573 and sea-water density of 1030 kg m^{-3}. Mean LGM ice-thickness is just over 1,172 m, 233 m greater

574 than that previously reconstructed by Hubbard et al. (2006) (Table 3). The modelled ice-sheet
575 surface rises to an elevation of c. 1850-1900 m along the central drainage divide, attaining a
576 maximum surface height of 2093 m around Öræfajökull, south of Vatnajökull.

4.2. Ice-sheet sensitivity

578 The LGM reference experiment was subject to a series of sensitivity experiments that explored, in
579 turn, the broad influence of individual parameters on ice sheet form and flow. The following
580 parameters and variables are explored: sea-level forcing; sensitivity to calving; sensitivity to sliding;
581 geothermal heat flux along with initial ice-sheet geometry (Table 3).

4.2.1. Inherited ice-sheet geometry

583 Given the limited availability of empirical data relating to Icelandic glaciation during MIS3, two
584 experiments were conducted to explore the influence of inherited ice-sheet geometry prior to the
585 'LGM' timeframe (26.5 - 19 ka: Clark et al., 2009). To achieve this the MAAT forcing curve was shifted
586 ±2°C from the reference experiment with imposed precipitation patterns left unchanged.

587 Despite very contrasting geometric trajectories during initial build-up, the two resulting ice sheets
588 closely match the dimensions of the reference experiment at the peak of the LGM, with areal and
589 volume differences of ≤3 % (Table 3). With the same deglaciation forcings, the ice sheet aligns once
590 more with the mass loss trajectories originally calculated in the reference experiment, revealing that
591 once the ice sheet reaches the shelf break in all sectors a state of equilibrium with the forcing
592 climate appears to be quickly reached.

4.2.2. Sea level and ice calving

594 Calving has a primary role in the stability of tidewater glaciers and marine ice sheets (Rott et al.,
595 2002; Rignot and Kanagaratnam, 2006; Howat et al., 2007; Rignot et al., 2010). Model sensitivity to
596 calving is thus explored through large-scale perturbations of the calving parameter (C) and also
597 through rescaling of the eustatic forcing curve by ±50 m. Reduction of sea level by a further 50 m
598 yields a slightly larger ice sheet (2.9 %) than the reference experiment. Conversely, an increase of
599 sea levels by 50 m leads to increased calving front losses and a restricted ice sheet that is reduced in
600 volume by 15 % at the LGM. Although the ice sheet still inundates the majority of the Icelandic
601 continental shelf, the mass losses at the ice margin influence ice thickness, with a concomitant ice
602 surface lowering of c. 4 %.

603 Order-of-magnitude changes in the calving parameter have a dramatic effect on the modelled ice
604 sheet. Increasing the calving parameter yields an ice sheet that is almost exclusively terrestrially
605 based, with corresponding volume and area reductions of 29 % and 22 % respectively. Conversely, a
606 lowered calving parameter value produces significant increases in area and volume by 17 % on the
607 reference experiment. However, ice expansion is limited primarily by the offshore bathymetry, since
608 beyond the continental shelf-edge the sea-floor is too deep for ice to remain grounded.
609 Furthermore, decreased sensitivity to calving leads to a slight net thinning of the ice sheet at its
610 maximal configuration, driven by ice-sheet expansion into marine sectors that are below the
611 equilibrium line, and thus more susceptible to surface melt processes – a somewhat counter-
612 intuitive result.

4.2.3. Sliding versus internal deformation

614 Whilst mass balance is the first-order control on ice-sheet growth and decay, ice-flow regime
615 determines the response, sensitivity, and overall ice sheet geometry (i.e., aspect ratio, volume and
616 hypsometry) particularly across marine sectors. Importantly, the partitioning of basal motion within
617 the ice-sheet model is linked to geothermal flux and melting at the ice-bed interface. Experiments
618 were thus conducted to explore the degree to which basal motion is critical to ice-sheet stability and
619 response time, and how altering the effective viscosity affects the ice sheet's ability to transport
620 mass from the interior to the margin. Where basal sliding occurs, its effectiveness is linked to bed

621 roughness; thus the higher the sliding parameter value, the easier ice can flow over obstacles at the
622 bed. Two experiments with order-of-magnitude change in the sliding parameter (A_{weert}) were
623 conducted.

624 A reduction of A_{weert} yields a stiffer (increased viscosity), thicker, less extensive ice sheet which has
625 much less mobility. Consequently, the ice sheet is less sensitive to external climatic forcing with a
626 supressed response and dampened fluctuations in lateral extent. In contrast, increasing A_{weert} by an
627 order of magnitude facilitates greater mobility and lateral expansion of the ice sheet through
628 increased flow, and results in a lower aspect ratio and mean ice thickness relative to the reference
629 experiment. The main impact of increased basal motion is increased sensitivity of a lower aspect ice
630 sheet to rapid fluctuations, particularly during deglaciation through accelerated flow and draw-down
631 of interior ice to the margins where surface melting, calving processes and the associated dynamic
632 feedbacks dominate.

4.2.4. Geothermal forcing
634 Changes in geothermal heat flux impact on modelled ice-sheet flow dynamics through their effect on
635 the zonation of subglacial thermal conditions (warm/temperate vs. cold/frozen) and hence the
636 distribution of basal motion. Four experiments examining the influence of the geothermal boundary
637 condition are conducted, using the following scaling values of the present-day geographical
638 distribution of geothermal heat flux: 1.5, 0.5, 0.25 and 0.1.

639 Increasing the present-day geothermal heat flux throughout the experiment causes negligible
640 dimensional change to the ice sheet (Table 3). The natural topographic barrier of the continental
641 shelf edge prevents any further significant expansion, and with an already low surface-aspect ratio in
642 the reference experiment, ice-sheet volume and thickness remain unchanged. Slight differences are
643 more apparent under geothermal flux reductions. Changes in ice sheet areal extent are generally
644 small, though values of maximum volume, and consequently mean thickness, tend to increase.
645 Under 10% scaling of the geothermal heat flux (range: 7-31 mW m^{-2}), the ice sheet mobility is
646 reduced resulting in a 4 % increase in volume, and 5 % thicker ice sheet than the reference
647 experiment.

648 Critically, changes in the geothermal heat flow to the ice-sheet bed has a significant impact on its
649 flow and drainage properties (**Figure 7**). Under the relatively warm geothermal conditions of the
650 present-day geothermal flux (Figure 2E) the ice sheet experiences constant basal melting, thereby
651 promoting stable and continuous fast-flow drainage and a relatively shallow ice-surface gradient.
652 Increases to the geothermal flux provide negligible changes, though by coupling a basal hydrological
653 system to the model further insights may be gained in this respect.. Conversely, with decreased
654 geothermal heating forcing, the spread of extensive cold-based ice induces dynamic instabilities,
655 causing rapid and dramatic switches in basal motion once basal conditions attain pressure melting
656 point during periods of climate amelioration. These flow cycles are increasingly vigorous when the
657 ice sheet is thinnest during the first 10 ka of ice build-up, with dramatic switching in ice discharge
658 varying by a factor of 4-5 on centennial timescales.

659 When geothermal fluxes are modified to values more closely aligned with background continental
660 fluxes (0.25G: 17-77 mW m^{-2}), the coverage of areas that could potentially host cold-based ice
661 become evident. If the present-day ice caps are ignored, where it has not been possible to
662 incorporate subglacial topographies, cold-based areas are abundant among the high relief of the
663 south-eastern and eastern fjords, the Tröllaskagi Highlands, and to a lesser extent the Vestfirðir
664 peninsula (Figure 6). For the latter, the pronounced geothermal hotspot across Snæfellsnes keeps
665 basal conditions persistently warm on this peninsula, particularly in the east (Figure 3E; Flóvenz and
666 Sæmundsson, 1993).

5. Discussion

5.1. Ice-flow directions and ice limits

Pre-LGM radiocarbon dates from Reykjanesskagi, which at this time would have been within the sub-aerially exposed Faxaflói indicate that the ice sheet probably traversed this peninsula c. 28 cal. ka BP (**Figure 1**A). From an initial ice-free domain, the modelled ice sheet is able to reach this coastline position within 7 ka of glaciation, expanding rapidly in response to strong precipitation input and the coalescence of five major ice nucleation centres over the four present-day ice caps and the Tröllaskagi Highlands. Limited relief over Vestfirðir leads to more subdued ice growth here that eventually becomes engulfed by the mainland ice sheet c. 29 ka BP. The close proximity of the southern shelf edge means the maximum ice-sheet extent in this sector is reached considerably early during the glaciation at c. 29 cal. ka BP. Elsewhere, the last terrestrial areas of Iceland to be overrun by ice include the tips of the Langanes, Vestfirðir (Látrabjarg) and Snæfellsnes peninsulas at 27.8 ka BP.

Growth of the modelled ice sheet continues synchronously up to the continental shelf edge to the north, east and west, reaching this position in all sectors by c. 23.7 ka BP. Here the IIS remains stable for the next 2 ka, reaching an absolute maximum extent at 22.9 ka BP, with significant retreat initiating after c. 21.8 ka BP. The total contribution to global eustatic sea-level rise at this time reaches a maximum value of 1.53 m

The symmetric nature of the ice sheet, as well its radial ice-discharge pattern, results in a very stable central ice divide that undergoes little migration throughout the entire glaciation. Isostatic deepening of the offshore troughs, coupled with the short isostatic response time of the crust (Sigmundsson, 1991), further stabilises the pattern of ice drawdown from the interior of the ice sheet into marine-based corridors.

Glacial lineations are a common landform signature of palaeo-ice sheets, indicative of fast, ice-streaming flow (Clark, 1993; Ó Cofaigh et al., 2002; Stokes and Clark, 2002; King et al., 2009), and have been readily identified across the Icelandic shelf to infer the presence of numerous ice streams that drained ice towards the shelf edge and an ice divide across central Iceland from east to west (Bourgeois et al., 2000; Stokes and Clark, 2001; Spagnolo and Clark, 2009; Principato et al., 2016). These flow sets mapped from Landsat satellite imagery and the Olex bathymetry database (**Figure 2**) reveal a good correspondence both on- and offshore (**Figure 8**), supporting the radial form and detailed flow pattern of the reference model experiment presented here. Closer analysis of modelled vectors reveals a pattern of flow adjustments through the latter stages of deglaciation. For example, ice flow towards Húnaflói and Héradsflói (sector 1 & 4 – **Figure 8**) both show an increased correspondence with the geomorphological record during the last major readvance of the ice sheet in the Younger Dryas. Such subtle variations in ice-sheet flow are typical of internal reconfigurations during ice-sheet thinning as ice divides adjust in response to the increasing influence of bed topography, though may also be a reflection of the greater abundance of empirical data reported onshore.

5.2. Ice-sheet collapse

At the LGM, 60% of the IIS was grounded below sea level, of which two-thirds (40% of the IIS) was grounded in water depths greater than 100 m (**Figure 4**). In terms of net contributions to global sea level, c. 53 % of the total 1.5 m s.l.e. of the maximum IIS came from grounded ice with a bed below sea level. Compared to ice cover over West Antarctica, the only present-day marine-based ice sheet, this contribution is much higher at 79 % (Fretwell et al., 2013). In both instances, these values highlight the sensitivity of both marine-based ice sheets to external fluctuations in oceanographic forcings such as sea-level or ocean temperature.

713 Limited dating suggests retreat of the IIS from the shelf was rapid, probably largely forced by
714 oceanographic drivers including rising sea-level and the northwards migration of the Polar Front
715 (Ingólfsson and Norðdahl, 1994, 2001; Andrews et al., 2000; Eiríksson et al., 2000; Jennings et al.,
716 2000; Geirsdóttir et al., 2002; Andrews, 2005, 2008; Norðdahl and Ingólfsson, 2015). The general
717 absence of submarine recessional-moraine sequences has been used to support this hypothesis,
718 though with few clear offshore topographic pinning points, deglaciation was probably predisposed
719 to unstable retreat (e.g. Dyke, 2004). The northwest sector (Vestfirðir) presents the single exception
720 to this generalised pattern, where several nested suites of large offshore moraines record local
721 grounded still-stands and/or readvances (**Figure 2**).

722 Surface-exposure (^{36}Cl) dating of bedrock and boulders from Vestfirðir suggests that the ice sheet
723 was thinning across the uplands here as early as 26.2 ka BP (Brynjólfsson et al., 2015). Although the
724 reference experiment fails to reproduce this early thinning necessary to expose nunataks on the
725 Vestfirðir peninsula, the absolute elevation of the ice surface was lowering from c. 24 ka BP in
726 response to the propagating isostatic depression of the crust. The isostatic response to ice-sheet
727 loading could therefore provide a mechanism by which nunataks emerge early above the ice-sheet.
728 Through rapid depression of the interior sectors of the ice sheet, the relative shift of the equilibrium-
729 line altitude up-glacier would subsequently expose far greater areas of the ice sheet to ablation
730 processes, potentially prior to any external climatic forcing.

731 From the maximal configuration at c. 21.8 ka BP, deglaciation occurs in two phases with distinctly
732 different styles. While initial instability is triggered by abrupt climate warming, subsequent retreat
733 ensues through disproportionate losses from calving (c. 45 % of total losses; Table 4; **Figure 9**).
734 Modelled ice retreat from the shelf edge to the present-day coastline is accomplished within 3.8 ka
735 along eastern sectors, and 5.0 ka in the west; the longer timeframe in accordance with the presence
736 of potential recessional moraines on the shelf in this sector, and possibly sustained by the
737 topographic influence of Vestfirðir nearby. The volumetric loss is significant, with average mass
738 wastage rates of c. 71 Gt a^{-1} between 21.8 ka BP to 18.0 ka BP - equating to a mean eustatic sea-level
739 contribution of 0.196 mm a^{-1}. For context, contemporary mass balance estimates for the West
740 Antarctic ice sheet and the Greenland ice sheet have been recently estimated at -102±18 and -
741 263±30 Gt a^{-1} respectively (Shepherd et al., 2012; Hanna et al., 2013). For the IIS, an ice sheet with a
742 maximum volume less than a third of the present West Antarctic Ice Sheet (Fretwell et al., 2013),
743 the implication is that once deglaciation initiated it was extremely rapid.

744 As climate amelioration continues and the ice sheet becomes progressively terrestrial based, a
745 switch in deglaciation style occurs, whereby surface melting begins to dominate the mass balance
746 regime. Topographic pinning points between the island's peninsulas halt the rapid retreat of the ice
747 sheet from the outer shelf at 16.3 ka BP, holding the ice margin in place until further abrupt warming
748 during the Bølling interstadial at 14.9 ka BP initiates a second ice-sheet-wide collapse. This phase of
749 rapid deglaciation is a common feature to all model experiments (**Figure 5**), with mass losses
750 occurring at a mean rate of 221 Gt a^{-1} over 740 years (melt >91 % of total losses; Table 4; **Figure 9**),
751 and resulting in a Late Weichselian minimum extent of 0.986 x 10^5 km^2 shortly after at 13.2 ka BP
752 (**Figure 4**).

753 A similar-style ice-sheet collapse event on the inner Icelandic shelf within a few centuries has been
754 inferred based on radiocarbon dates of c. 15.0 cal. ka BP in Jökuldjúp and 14.8 cal. ka BP from the
755 150 m high marine limit at Stóri-Sandhóll, west Iceland (Jennings et al., 2000; Ingólfsson and
756 Norðdahl, 2001; Principato et al., 2005) (**Figure 1**B). Various factors have been suggested to account
757 for this dramatic 125 km retreat inland, including a contemporaneous and rapid eustatic sea-level
758 rise during MWP-1A, in combination with a short-lived temporal equilibrium between glacio-isostatic
759 uplift and sea-level rise (Norðdahl and Ingólfsson, 2015). While the marine-terminating ice sheet
760 would have undoubtedly been sensitive to rapid fluctuations in oceanic forcings, the model clearly

relates rapid retreat at this time to atmospheric warming significantly elevating the equilibrium-line altitude. The surface area of the ablation zone across the ice sheet rises from 35% to 83% in just 500 years (.

Figure 10), this dynamic further intensified by the rapidly responding isostatic rebound of the crust at this time.

The isostatic adjustment scheme coupled to the ice-sheet model (in this study) predicts that the greatest depression during the LGM probably occurred over northwest Iceland. This area coincides with the areas of greatest ice thicknesses at the LGM, in the major topographic lows of Breiðafjörður and Húnaflói close to the central ice divide (**Figure 11**). Isostatic adjustment values at this time equate to c. 200 m depression below the present-day level, far from the 570 m of depression predicted by Norðdahl & Ingólfsson (2015) at the present-day coastline using steady-state equations. Further discrepancies in southern Iceland between the position of the modelled coastline and the marine ice-contact deltas found in the Búði moraine complex at the time of the Younger Dryas (**Figure 12**) (Geirsdóttir et al., 1997) indicate that isostatic depression is underestimated within the reference experiment. Considering uplift rates during deglaciation reached as high as 107 mm a^{-1} (Rundgren et al., 1997), the acute sensitivity and heterogeneity of crustal deformation around Iceland makes this a clear challenge for ice-coupled modelling. Accurate reconstruction of relative sea-level curves and uplift rates would therefore be best resolved through explicit Glacial Isostatic Adjustment (GIA) modelling, whereby independent predictions of ice thickness can be incorporated to explore the full range of viable Earth rheology parameters (e.g., Auriac et al., 2013).

5.3. Ice sheet aspect ratio
The collection of numerous cosmogenic-exposure age dates from table mountains within the neovolcanic zone (Licciardi et al., 2007) provides valuable constraints with which to reconstruct the surface-aspect ratio and slope of the retreating ice sheet. While these dates are limited to two discrete time intervals during deglaciation related to episodes of high volcanic activity (c. 14.4 - 14.2 ka and 11.1 - 10.5 ka), the data consistently predict a low aspect-ratio ice-sheet surface with slope gradients between 1:125 and 1:180. The geometry of the reference modelled ice sheet presented here reproduces similar shallow surface gradients of between 1:172 and 1:192 during deglaciation (**Figure 13**) providing verification that the mass-balance and flow regime are broadly correct and consistent.

North of Vatnajökull, during the Bølling climatic oscillation at 14.7 ka BP, the modelled ice sheet overruns the isostatically adjusted table mountain summits of Bláfjall and Gæsafjöll by c. 400 m, more than the 15 % of the total thickness as suggested by Smellie (2000) necessary for their subglacial formation. The modelled ice sheet margin falls 10 km short of Snartarstaðarnúpur, though the low elevation of this mountain indicates that ice cover was probably not particularly thick here when it last erupted. Differences southwest of Langjökull are more pronounced due, in part, to conflicting interpretations of the extent and form of the Younger Dryas ice sheet. The reference model extent was largely constrained in this sector by the large Búði moraine complex (**Figure 1**) (Geirsdóttir et al., 1997, 2000). Dated table mountain summits outside of this limit (e.g. Geitafell and Hvalfell), contradict this interpretation, indicating that ice extent was possibly much greater at this time. On discussion of their samples, Licciardi et al. (2007) noted that any snow or rime-ice shielding over the mountain summits could increase the reported ages by up to 18%. Though this may not be sufficient to account for differences in the modelled ice extent, it raises the possibility that mountains near the margin of the ice sheet may have hosted persistent and independent ice fields during the Younger Dryas stadial.

Modelled ice surface slopes are even shallower within the ice-sheet interior during the maximal configuration (> 1:208), comparable with slope measurements from the present-day Greenland and Antarctic ice sheets (cf. Bamber et al., 2013; Fretwell et al., 2013). Despite this, the modelled

809 Icelandic ice sheet is still sufficiently thick to override previously assumed nunataks, such as in the
810 Tröllaskagi highlands (Norðdahl, 1983), and on Vestfirðir and Skagi (Principato and Johnson, 2009).
811 Based on palaeo-analogues in other glaciated regions (e.g. Ballantyne, 2010; Fabel et al., 2012), the
812 assumption that the erosional (trimline) boundaries mapped in Iceland represent palaeo-ice surfaces
813 is worthy of re-examination in the context of the shelf-edge glaciation model presented here.

5.4. The Younger Dryas

814
815 The reference model experiment of the Younger Dryas Stadial presented is in good agreement with
816 leading interpretations from the empirical record, with ice margins restricted largely to the present-
817 day terrestrial landmass (**Figure 12**). Truncated raised marine shorelines in the mouths of fjords and
818 major valleys around Iceland demonstrate that the Younger Dryas ice sheet expanded across many
819 coastal sites that had been ice-free since the Bølling deglaciation (~14 cal. ka BP) (cf. Ingólfsson et al.,
820 2010). For example, large outlet glaciers filled the largest northern fjords of Skagafjörður, Eyjafjörður
821 and Skjálfandi (Norðdahl and Haflidason, 1992; Norðdahl and Pétursson, 2005), draining ice from the
822 main central ice-divide. However, occurrences of the Skógar-Vedde tephra in ice-dammed lake
823 sediments in Fnjóskadalur show that numerous ice-free enclaves existed in north central Iceland at
824 this time (Norðdahl and Haflidason, 1992). This evidence indicates that the modelled ice sheet
825 reconstruction could be generally too thick in this sector. Furthermore, truncated shorelines on the
826 Langanes Peninsula also reveal that only the easternmost part of the peninsula was probably ice-free
827 during the YD (Pétursson, 1991; Norðdahl and Hjort, 1995). However, model experiments
828 consistently fail to glaciate this northeastern sector due to the long distance from the nearest
829 accumulation centre around present-day Vatnajökull.

830 Northeast of Reykjavík at Helgafellsmelar, the termination of the Younger Dryas glacial advance is
831 marked by ice-contact deltas and related shoreline features radiocarbon dated to 11.8 cal. ka BP
832 (Ingólfsson et al., 1995). However, this position is difficult to reconcile with an apparent Younger
833 Dryas ice limit also constrained by the Búði moraine complex ~100 km to the east (cf. Norðdahl et
834 al., 2008). In light of this evidence, it is probable that local (semi) independent ice fields persisted on
835 the higher terrain of Reykjanesskagi throughout the Younger Dryas stadial (e.g., Geirsdóttir and
836 Eiriksson, 1994).

5.5. Geothermal forcing

837
838 A major question regarding the LGM configuration is the extent of ice cover on Vestfirðir and its
839 association with the mainland ice sheet. Geomorphological features such as preserved upland block-
840 fields, arêtes and old ^{36}Cl dates have been used to infer the presence of extensive cold-based ice or
841 minimal glacial erosion here during the LGM (Principato et al., 2006; Brynjólfsson et al., 2015).
842 Model experiments presented here appear to contradict the empirical record in this respect due to
843 the effect of the large geothermal fluxes recorded from eastern Vestfirðir encouraging permanent
844 subglacial melt in this sector (Figure 3E; Flóvenz and Sæmundsson, 1993). By reducing the
845 geothermal flux to nearer background continental values, basal thermal partitioning does indeed
846 become more pronounced, with upland areas remaining frozen for up to 45% longer during
847 glaciation (**Figure 6**). Given the sensitive nature of the ice sheet to the geothermal boundary
848 condition, it appears further data concerning the heterogeneous distribution of the geothermal flux
849 across Iceland are necessary before accurate modelling of the basal thermal regime can be achieved.

850 At the broad scale, model experiments confirm that geothermal heat gradients can exert a primary
851 influence on ice sheet sensitivity and dynamic response. For the IIS, increased geothermal heat
852 supply to the ice-bed interface plays a minor role on ice growth trajectories (Table 3), which is
853 ultimately restricted by the continental shelf edge. However, it is reductions in geothermal forcing to
854 values closer to those measured over ancient continental shields that lead to the most notable
855 changes in its behaviour.

856 The predominant response is the shift from persistent pressure melting induced at the base of the
857 ice sheet to a cyclical phasing of ice-stream shutdown and reactivation on sub-millennial timescales
858 (**Figure 6:** Spatial partitioning of basal temperatures through the Late Weichselian glacial cycle under
859 various geothermal flux scenarios. Dark green areas are more likely to be warm based throughout
860 the glaciation, while purple regions more likely to be cold based. Regions beneath the present-day
861 ice caps are masked, as data relating to their subglacial topographies were not included in the ice
862 flow model and therefore basal conditions here are not calculated accurately.

863 **Figure 7Figure 7**). The timing and dynamics of these flow-phasing events are determined through a
864 combination of basal thermomechanical switching spatially propagated and amplified through
865 longitudinal coupling. However, it is the major oscillations within the NGRIP climatic record used to
866 force the model that modulate the main phases of streaming activity. Relatively thin ice-sheet outlet
867 glaciers, particularly those terminating in marine sectors, are most sensitive to these changes where
868 advection of warmer ice through the ice-mass is rapidly achieved, inducing basal melting and
869 subsequent fast-flow. Such dynamic behaviour resonates with other modelling studies showing that
870 basal ice temperatures are highly sensitive to relatively small changes in geothermal heat flow
871 (Greve and Hutter, 1995; Siegert and Dowdeswell, 1996; Tarasov and Peltier, 2003; Greve, 2005).

872 In previous studies where spatially varying geothermal heat-flow distributions have been used,
873 modelled ice-sheet reconstructions have shown significant sensitivity and variation (e.g. Näslund et
874 al., 2005; Rogozhina et al., 2012). For palaeo-ice sheets where geothermal heat flow is relatively
875 heterogeneous, or dominated by relatively low continental flux values, the implication for transient
876 dynamic behaviour is significant. Examples include the eastern Laurentide and northern
877 Fennoscandian ice sheet sectors, flowing over bedrock largely composed of Caledonian-age
878 crystalline lithologies. Borehole measurements in these regions have revealed low geothermal heat
879 fluxes of < 34 mW m^{-2} (Lubimova et al., 1972; Kukkonen, 1989; Rolandone et al., 2003). The
880 increased sensitivity of the ice sheet to thermal conditions at the ice-bed interface partly explains
881 the resulting unstable dynamics, or ice-stream purges, that have been inferred for these sectors
882 during deglaciation under a rapidly changing climate (e.g. MacAyeal, 1993; Papa et al., 2005;
883 Winsborrow et al., 2010). Moreover, geothermal hotspots have been identified beneath the current
884 Polar ice sheets, including the Northeast Greenland ice stream (Fahnestock et al., 2001), and the
885 Siple Coast, West Antarctica (Engelhardt, 2004; Winberry and Anandakrishnan, 2004; Corr and
886 Vaughan, 2008), where the first direct measurement of geothermal heat flux has been recorded at
887 285 ± 80 mW m^{-2} beneath the Whillans ice stream (Fisher et al., 2015) – comparable with the upper
888 range of fluxes within the current Icelandic neovolcanic zone. The implications of our findings for ice-
889 stream stability and rapid ice sheet drawdown are thus significant for determining scenarios of
890 future non-linear deglaciation.

891 ## 6. Conclusions
892 - Limited empirical data from a variety of sources indicate that an extensive marine-based ice
893   sheet occupied the Icelandic continental shelf between 28.1 – 15.4 cal. ka BP. Although
894   chronological constraints are poorly distributed, the offshore glacial geomorphological
895   footprint described here indicates that the Icelandic ice sheet probably reached the
896   continental shelf edge in all sectors during the Last Glacial Maximum before rapidly
897   collapsing.
898 - In this paper we incorporate coupled climate-flow modelling to examine this concept of a
899   shelf-wide Late Weichselian Icelandic Ice Sheet within the context of available empirical
900   constraints, providing a robust reconstruction that describes the growth and subsequent
901   deglaciation trajectory through to the Younger Dryas and Early Holocene.
902 - The maximum areal extent of the reference ice sheet is almost double the previous
903   reconstruction by Hubbard et al. (2006) at 5.62 x 10^5 km^2. Due to the primary influence of
904   geothermal heat supply on the dynamics of the Icelandic ice sheet, a low aspect ratio is

905   maintained with a mean thickness of 1172 m and volume of 6.58 x 10^5 km^3 at the LGM,
906   equivalent to 1.53 m of eustatic sea level.

907 • At the LGM, 60 % of the Icelandic ice sheet was grounded below sea-level, bounded across
908   all sectors by an active calving margin that extended to the continental shelf break. During
909   subsequent deglaciation the retreat rate of this marine-based ice sheet was rapid, losing
910   mass at a mean rate of 71 Gt a^{-1} between 21.8 and 18.0 cal. ka BP.

911 • Once pinned on the present-day coastline, the ice sheet underwent a second more abrupt
912   phase of collapse at the start of the Bølling-Allerød interstadial (GI-1e), losing mass at a
913   mean rate of 221 Gt a^{-1} over the course of c. 750 years, forcing retreat of the ice sheet firmly
914   into terrestrial sectors. The bulk of mass loss during this period comes from surface melt in
915   response to climate warming, forcing a widespread increase in the elevation of the
916   equilibrium-line altitude and exacerbated by the already low aspect-ratio of the ice surface.

917 • While the areal extent of the ice sheet has a strong topographic control, ice thickness and
918   volume respond dramatically to long-term changes in the basal thermal regime, and
919   consequently the effective mobility of the ice sheet. Reduced geothermal heat flow to the
920   ice-bed interface increases the sensitivity of marginal sectors to cycles of centennial-scale
921   fast-flow conditions. These are in turn are modulated by transitions from cold to warm
922   phases of the NGRIP temperature forcing curve.

923 • The major influence that basal geothermal heat supply imparts on ice-sheet flow dynamics
924   suggests that further work is required to explore the role of this transient boundary
925   condition. Adopting a fully coupled ice-lithosphere-mantle model, in addition to the
926   introduction of a subglacial hydrology layer, would provide further insight into the
927   behaviour, evolution and feedbacks between ice sheets and their geothermally active beds.

928

Acknowledgements

Figure captions

Figure 1: A) Suggested limits of the last Icelandic Ice Sheet based on geophysical data observations, alongside radiocarbon dates (cal. ka BP) constraining an upper age for Late Weichselian glacier expansion (red) and radiocarbon dates from probable reworked sediments (yellow) (cf. Table 1). B) Key radiocarbon dates constraining deglaciation of the Late Weichselian ice sheet, alongside the speculated limits of the Younger Dryas glacier expansion (Pétursson et al., 2015). The present-day neovolcanic zone is characterised by relatively high geothermal heat fluxes and volcanic eruptions, forming part of the active Mid-Atlantic lithosphere boundary.

Figure 2: A) Overview of the glacial geomorphology of the Iceland continental shelf (Spagnolo and Clark, 2009), corroborated and supplemented with additional landform mapping from Landsat satellite imagery (onshore) and the EMODnet DTM (offshore – dark colours). Increased bathymetry data coverage to the northwest in particular reveal a number of newly identified glacial landforms close to the shelf edge. Trough extents are delimited as local topographic lows relative to the surrounding terrain. Flow sets onshore are grouped according to flow direction affinity and contiguity. B) Bathymetric profile over a prominent moraine ridge close to the northern shelf edge.

Figure 3: Model boundary conditions, climatic values derived from multiple regression analysis in Table 2. A) Mean January temperature, B) Mean July temperature, C) Mean annual precipitation, D) Melded topographic datasets, E) Geothermal heat flux - circle radii are scaled to the geothermal flux from each borehole, and F) Names and locations of the present day ice caps across Iceland. The blue arrow indicates the starting longitude and direction of the positive west-east precipitation gradient applied within the reference experiment.

Figure 4: Selected time slices showing surface-ice velocities between 31.0 and 11.7 ka BP from the reference model experiment. Compared to the reconstruction of Hubbard et al. (2006 shown in light blue, maximum expansion to the north, east and west is evident during the LGM.

Figure 5: Areal and volumetric sensitivity of the optimal experiment to magnitude changes in model parameter values. Abbreviations: A_{weert} (sensitivity to sliding), C (sensitivity to calving), SL (relative sea level), and T (mean annual air temperature prior to 28.5 ka BP).

Figure 6: Spatial partitioning of basal temperatures through the Late Weichselian glacial cycle under various geothermal flux scenarios. Dark green areas are more likely to be warm based throughout the glaciation, while purple regions more likely to be cold based. Regions beneath the present-day ice caps are masked, as data relating to their subglacial topographies were not included in the ice flow model and therefore basal conditions here are not calculated accurately.

Figure 7: The effects of scaled present-day geothermal forcing on the mean basal velocity of the ice sheet through the last glacial cycle. Centennial-scale thermomechanical switching, modulated by transitions in the climate forcing from relatively warm to cold conditions, become more apparent with reductions in the supply of heat to the base of the ice sheet. Increases beyond the present-day geothermal flux have negligible effects on the mean basal velocity regime.

Figure 8: Modelled basal velocity vectors (red) versus observed orientations of mapped glacial lineations (blue) on- and offshore during various stages of modelled ice retreat at 22.9, 14.7 and 11.7 ka BP. Notable examples of improved flow correspondence through deglaciation include group i offshore, and flow sets 1 and 4 onshore.

Figure 9: Mass turnover (Gt a^{-1}) and volume changes of the modelled Icelandic Ice Sheet through the Late Weichselian. Two periods of intensive deglaciation post-LGM are indicated, with greatest mass losses occurring during the climate warming of the Lateglacial interstadial. Greenland Interstadials

982 are defined by the INTIMATE event stratigraphy (Rasmussen et al., 2014), and climate forcing
983 applied through a scaled version of the NGRIP ice-core record (Section 3.1) (Andersen et al., 2004).

984 **Figure 10:** A) Changes in the proportion of the ice surface experiencing surface melting over a period
985 of 500 years, leading to rapid retreat of the ice sheet during the Lateglacial interstadial; B-C) Sharp
986 rises in the mean annual air temperature at this time led to more intensive surface melting at the ice
987 sheet margins.

988 **Figure 11:** Ice thicknesses at the Last Glacial Maximum, showing thickest ice cover over the
989 Breiðafjörður and Húnaflói. Present-day topography above 1 km a.s.l. (including the present-day ice
990 caps) is indicated in black.

991 **Figure 12:** Surface velocities of the modelled Younger Dryas ice sheet, with the contemporary
992 coastline calculated from isostatically adjusted topography. The ice sheet at this time reached a
993 maximum elevation of c. 1750 m a.s.l. Speculated empirical limits for glacial extent at this time
994 (black line) are shown for comparison (Pétursson et al., 2015).

995 **Figure 13:** Transects through the neovolcanic zone (inset – red) indicating locations of cosmogenic-
996 exposure dated table mountains and modelled ice-sheet profiles from the reference experiment
997 through deglaciation. Dated table mountains from Licciardi et al. (2007) include: (Bl) Bláfjall, (Bú)
998 Búrfell, (Gæ) Gæsafjöll, (Ge) Geitafell, (Ha) Hafrafell, (He) Herðubreið, (Hö) Högnhöfði, (Hv) Hvalfell,
999 (R) Rauðafell, (Sk) Skriða, and (Sn) Snartarstaðarnúpur.
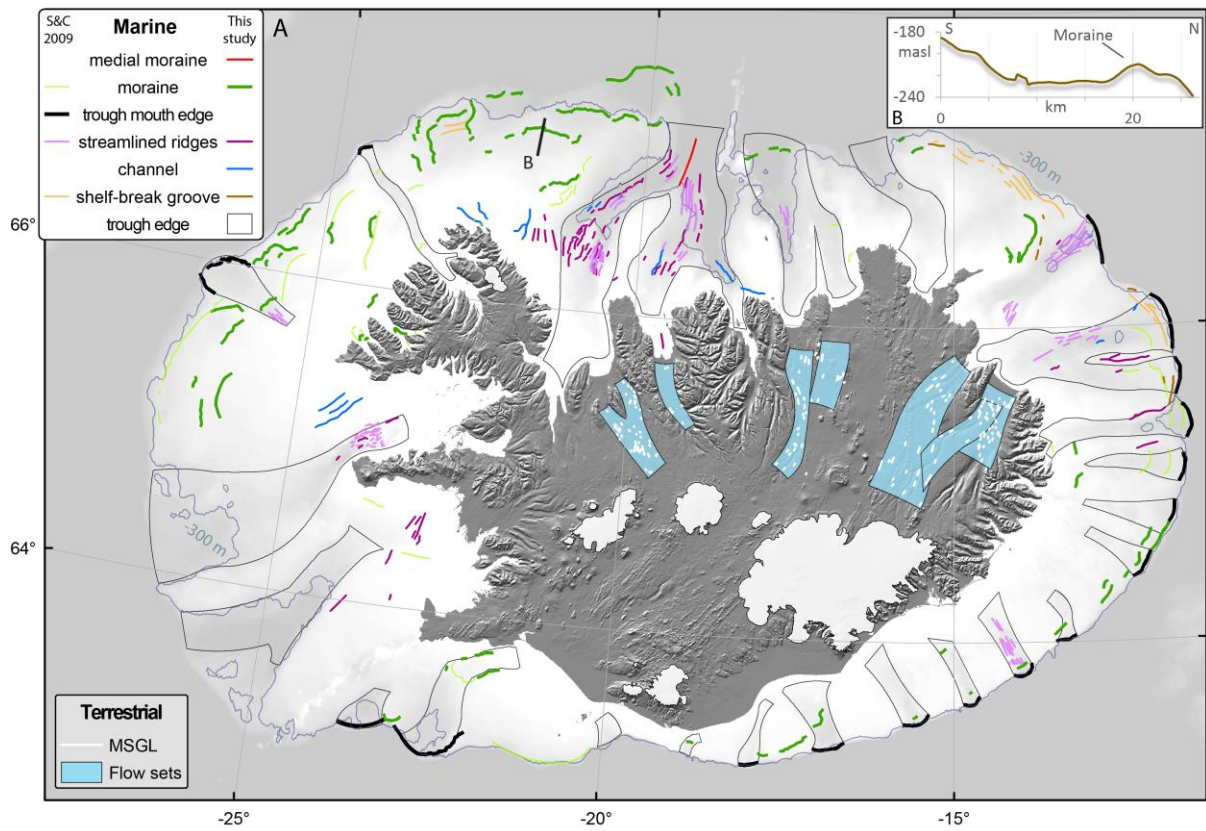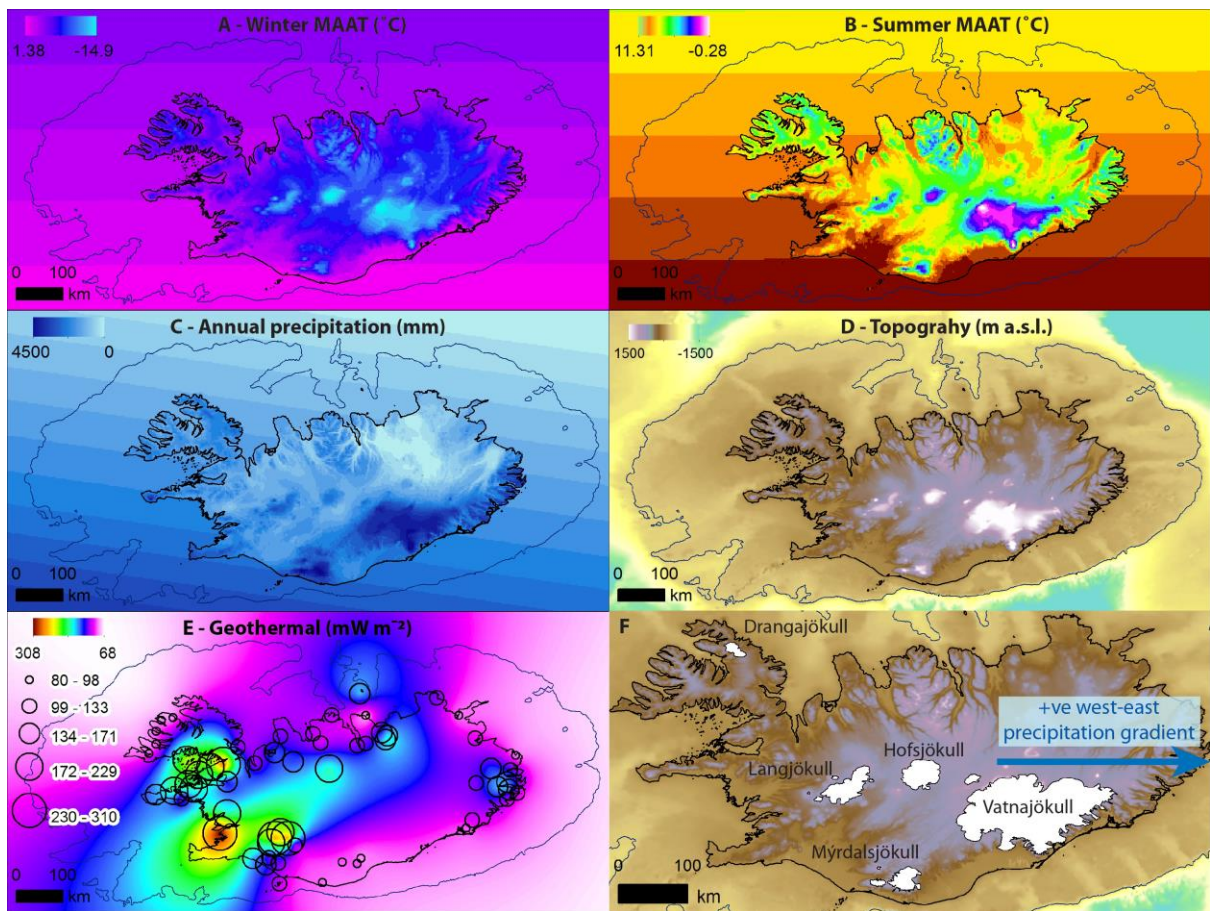
1000
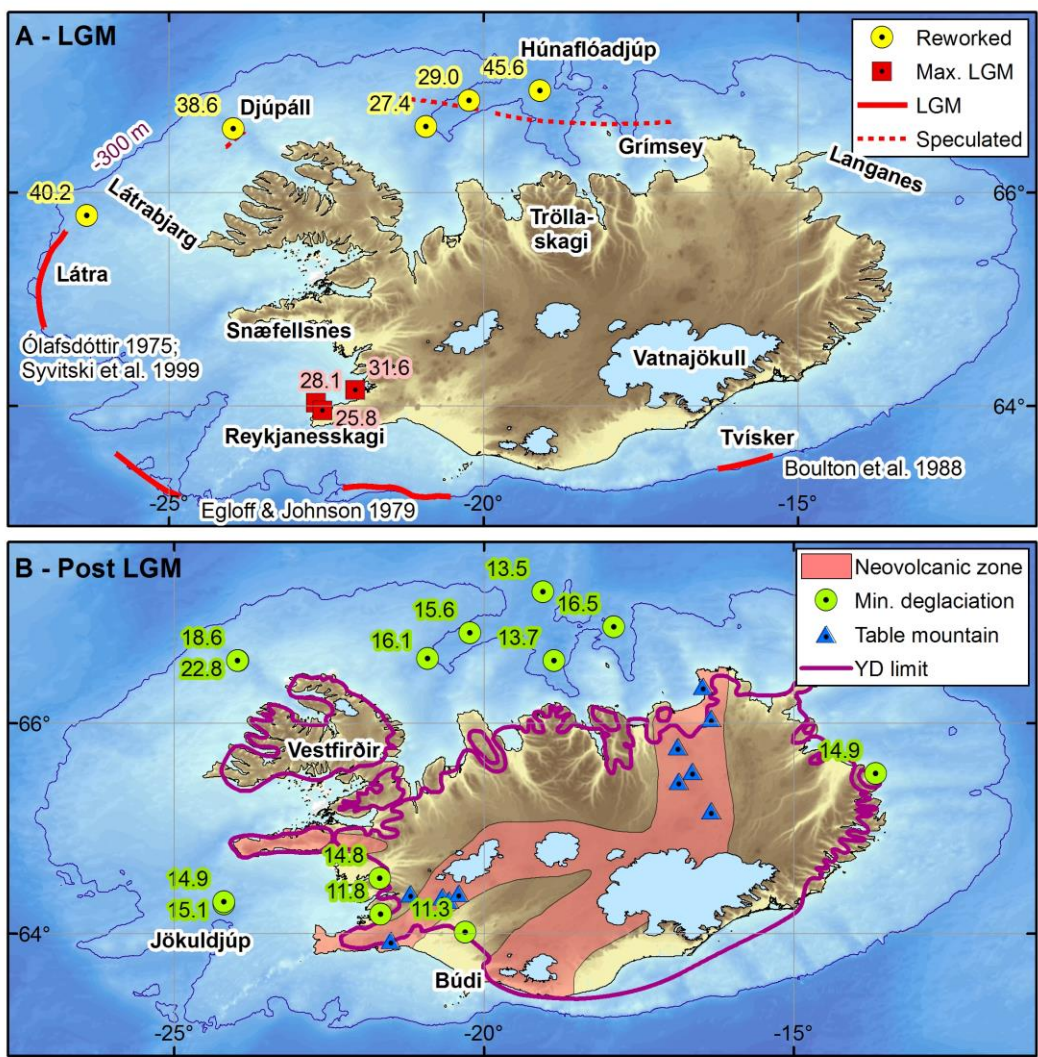
Figure 1

1004   Figure 2
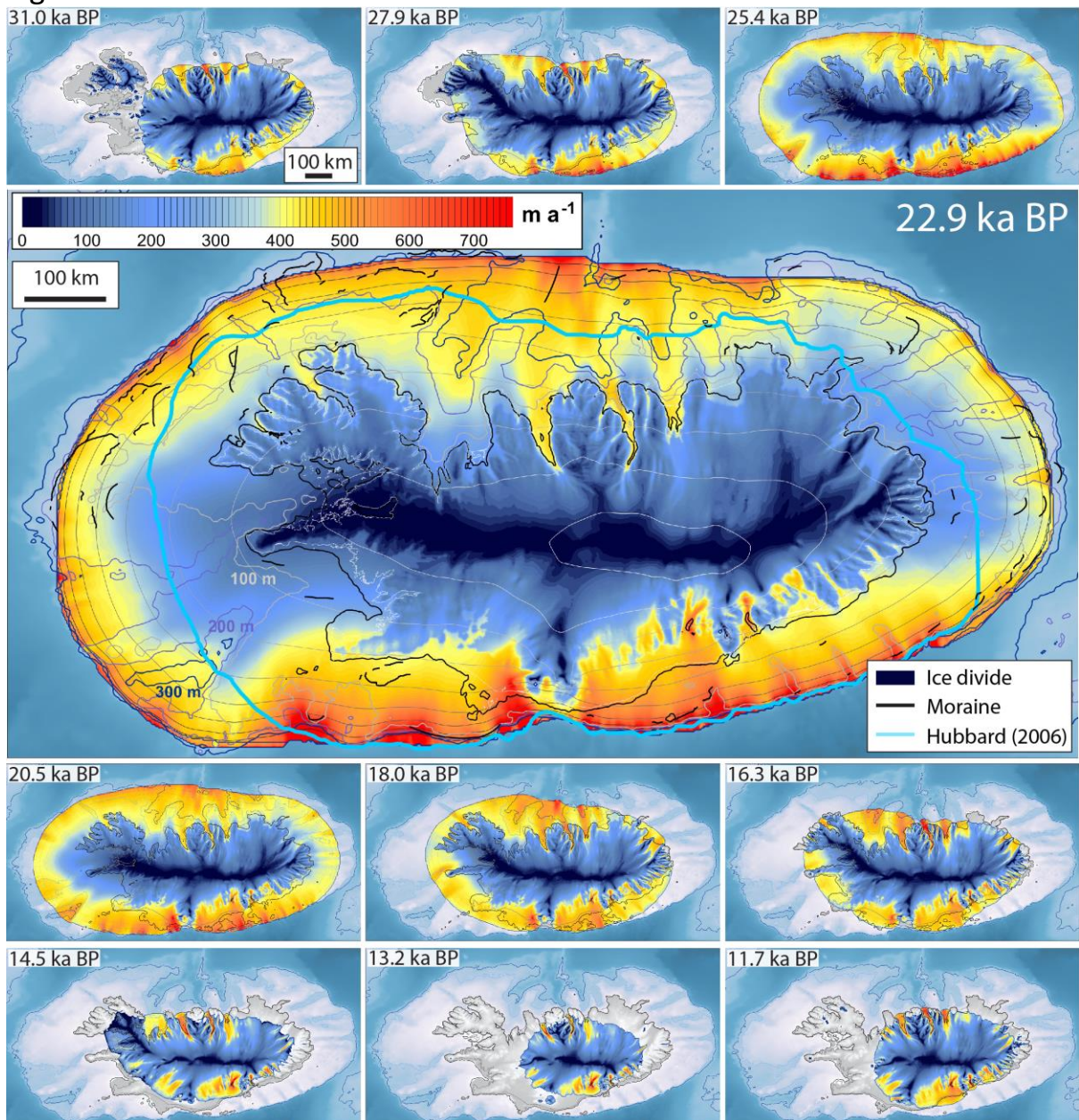

1005

1006

1007   Figure 3

1008

1009

1010   Figure 4

1011

1012

1013   Figure 5
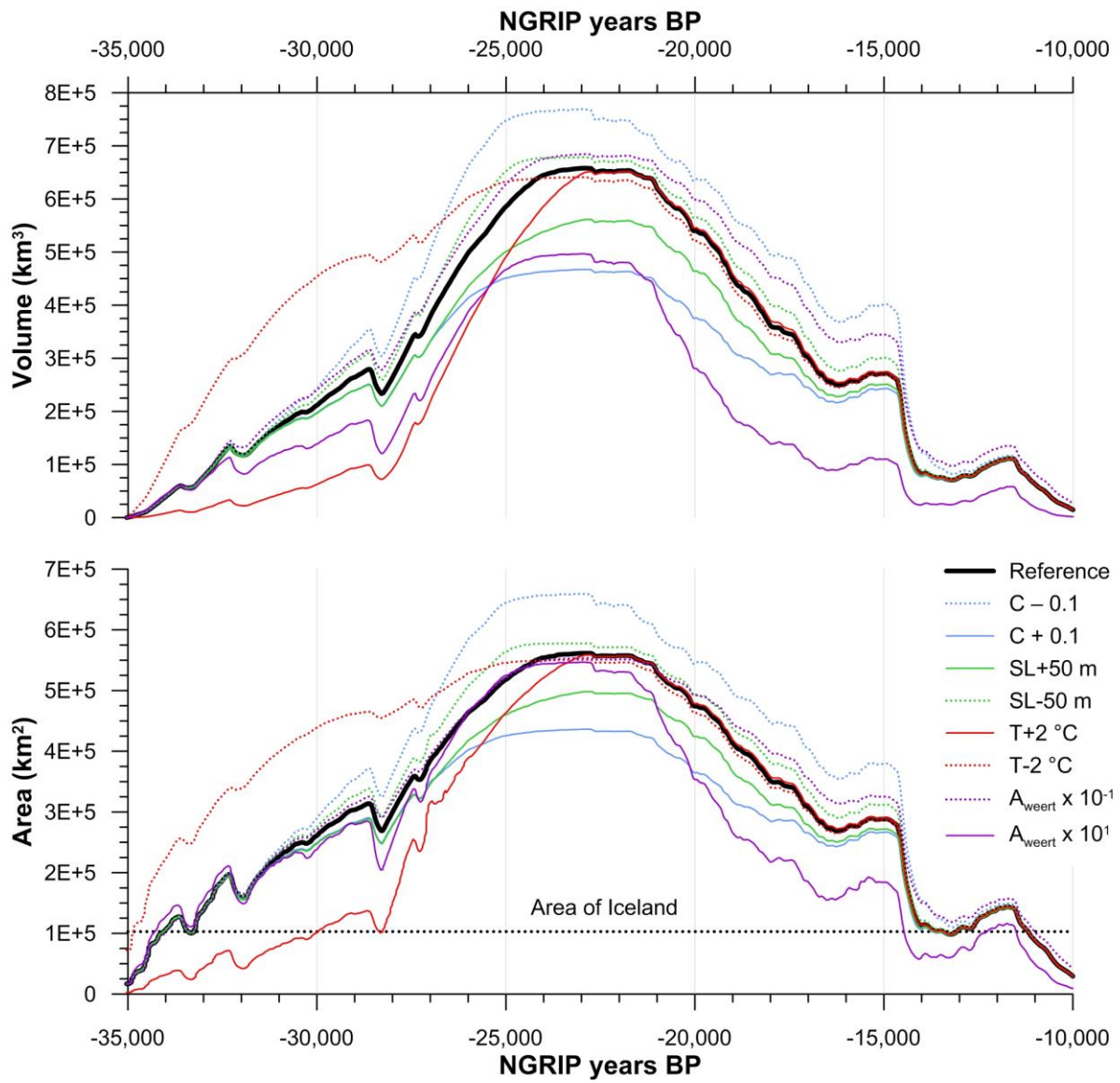
1014

1015

1016   Figure 6
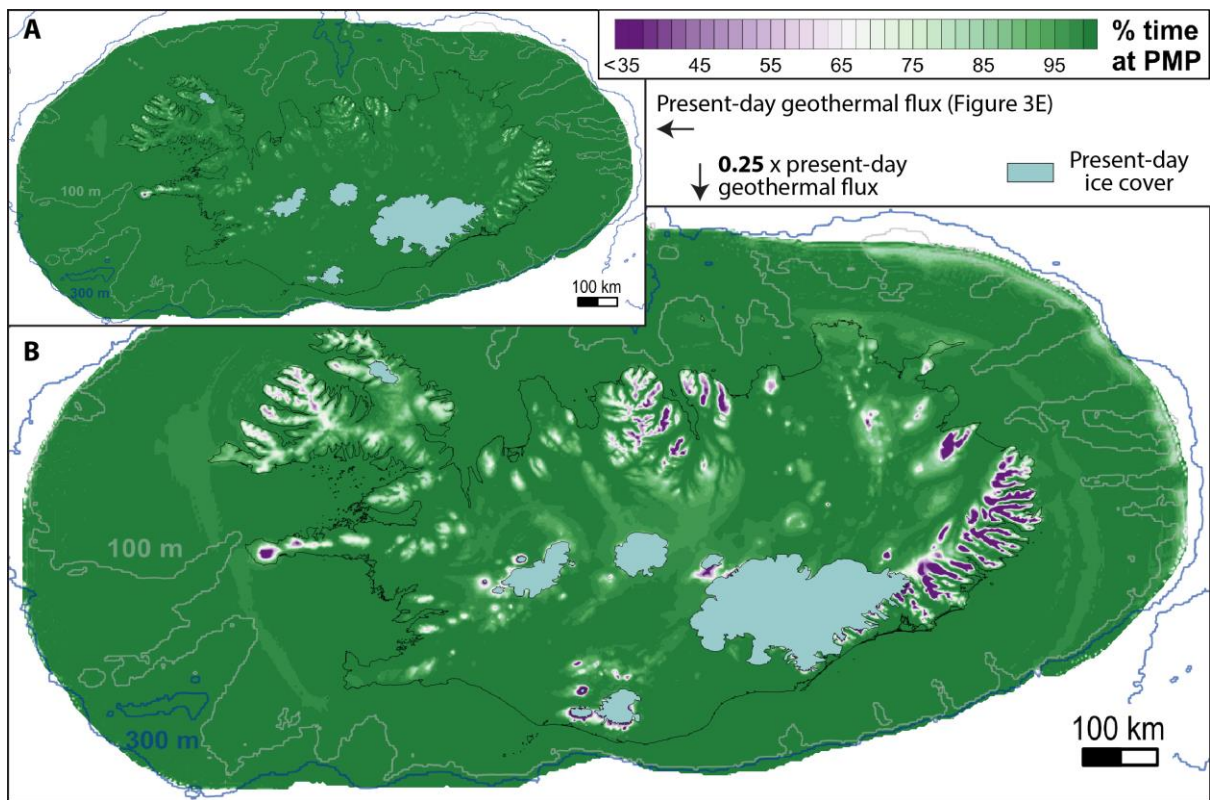
1017

1018

1019   Figure 7
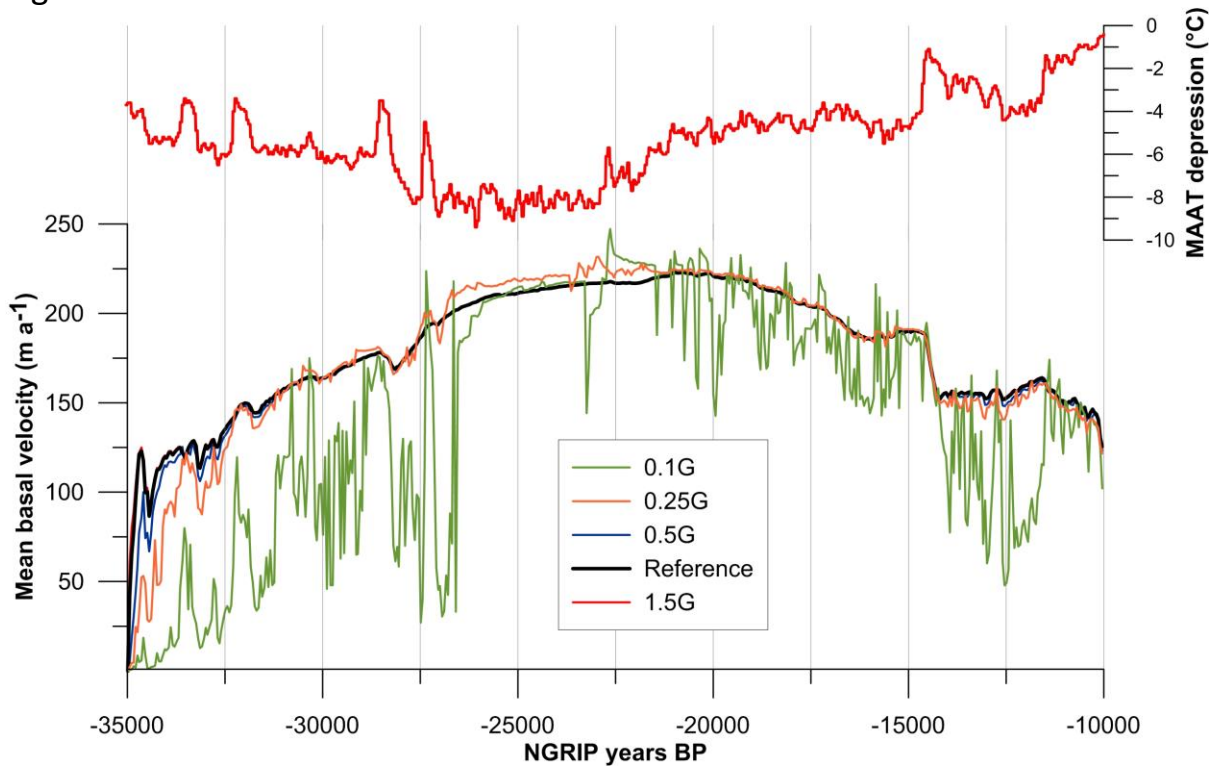
1020

1021
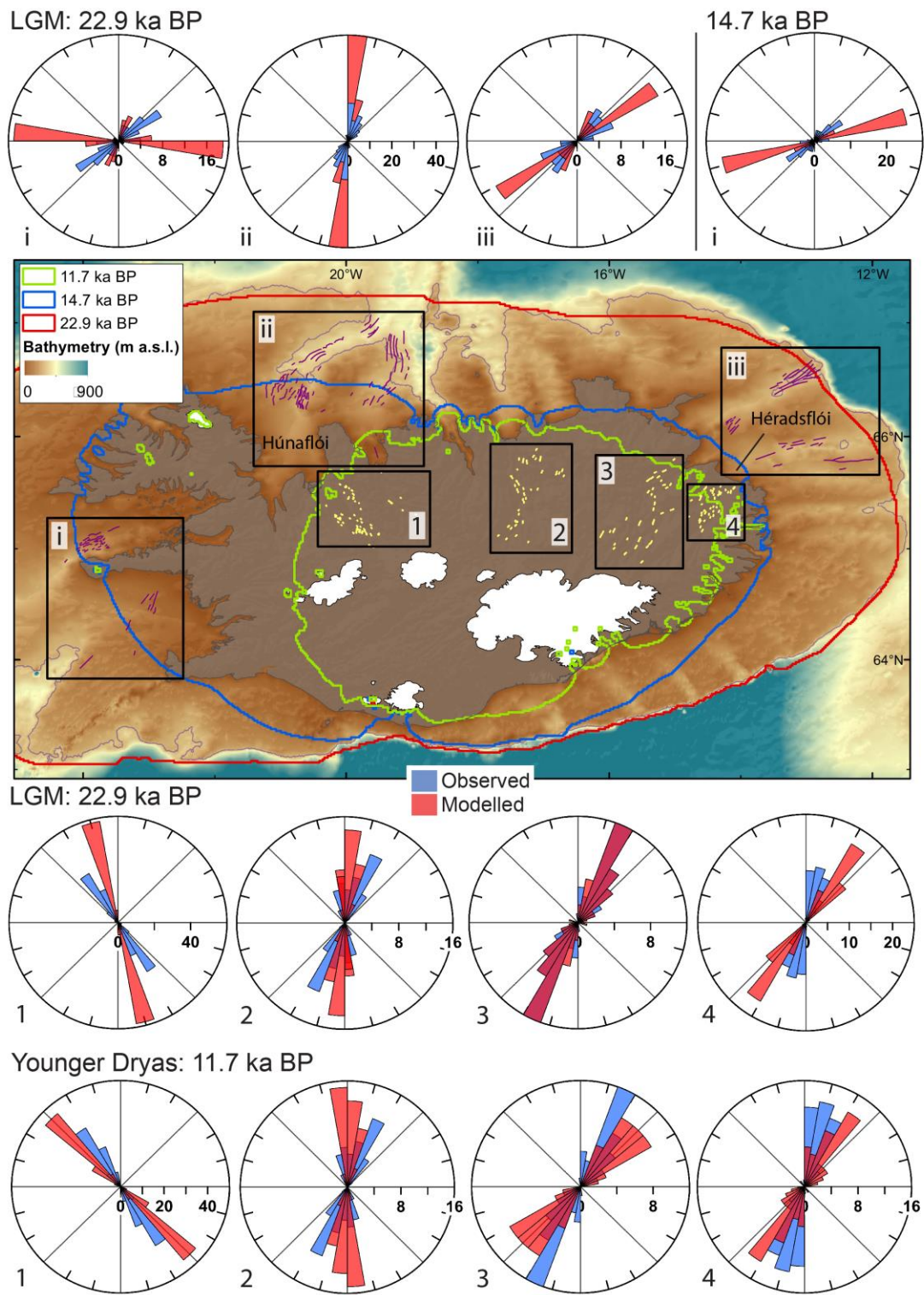
Figure 8

1025   Figure 9
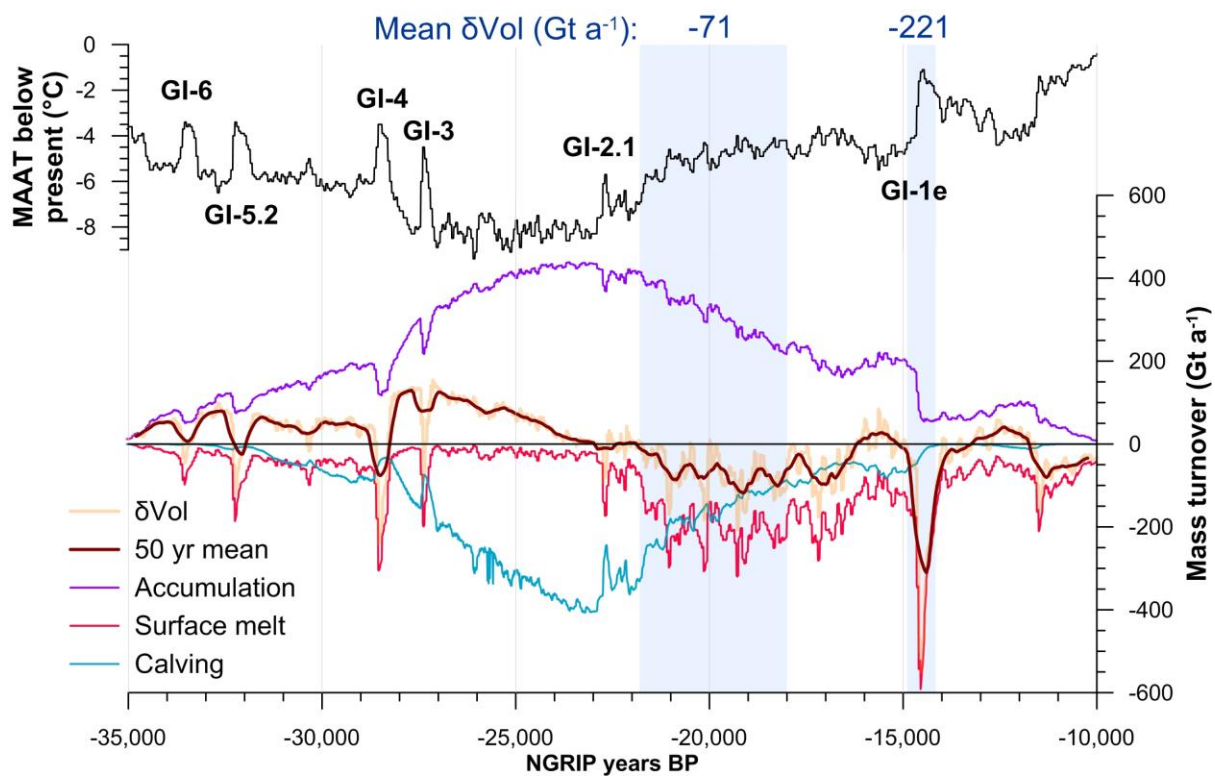
1026

1027

1028   Figure 10
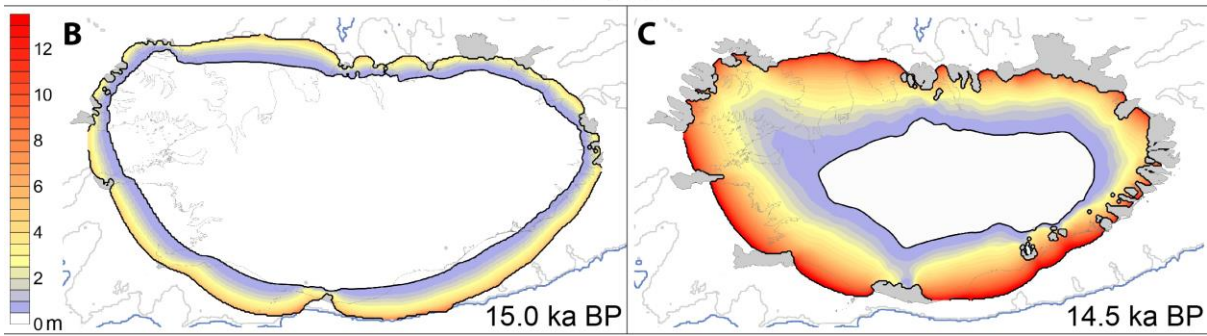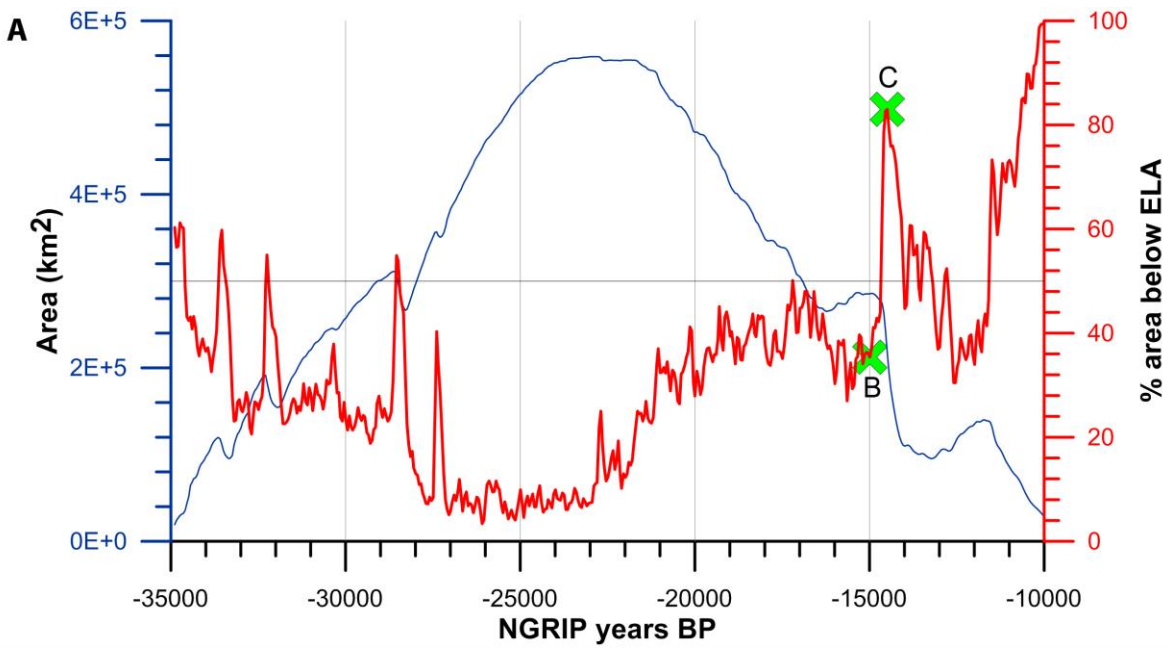
1032   Figure 11
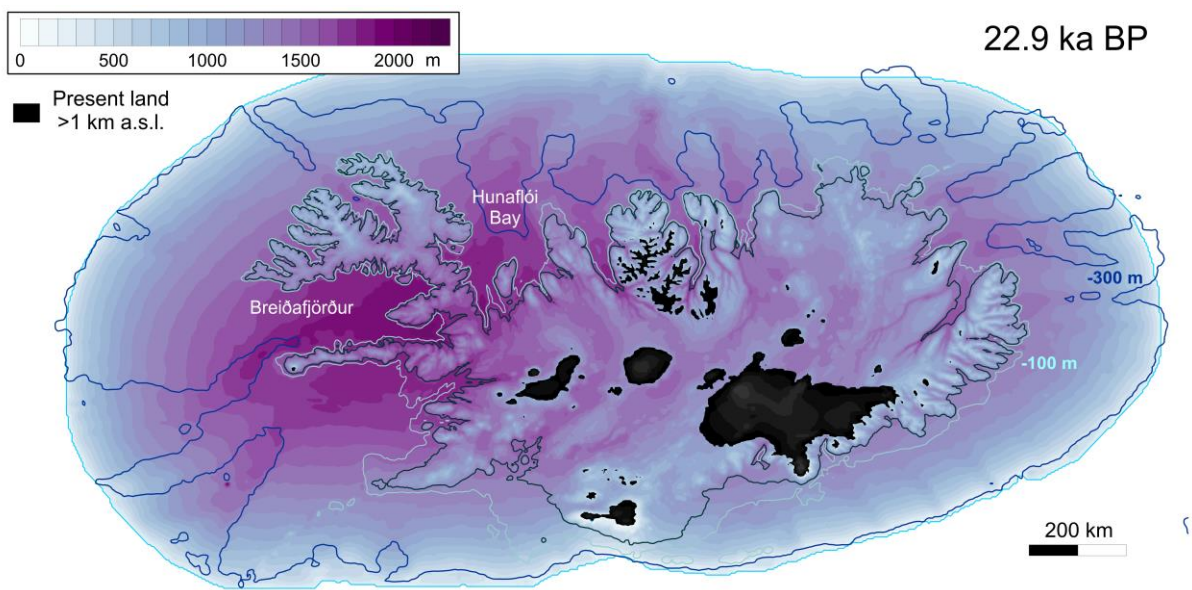
1033

1034

1035   Figure 12
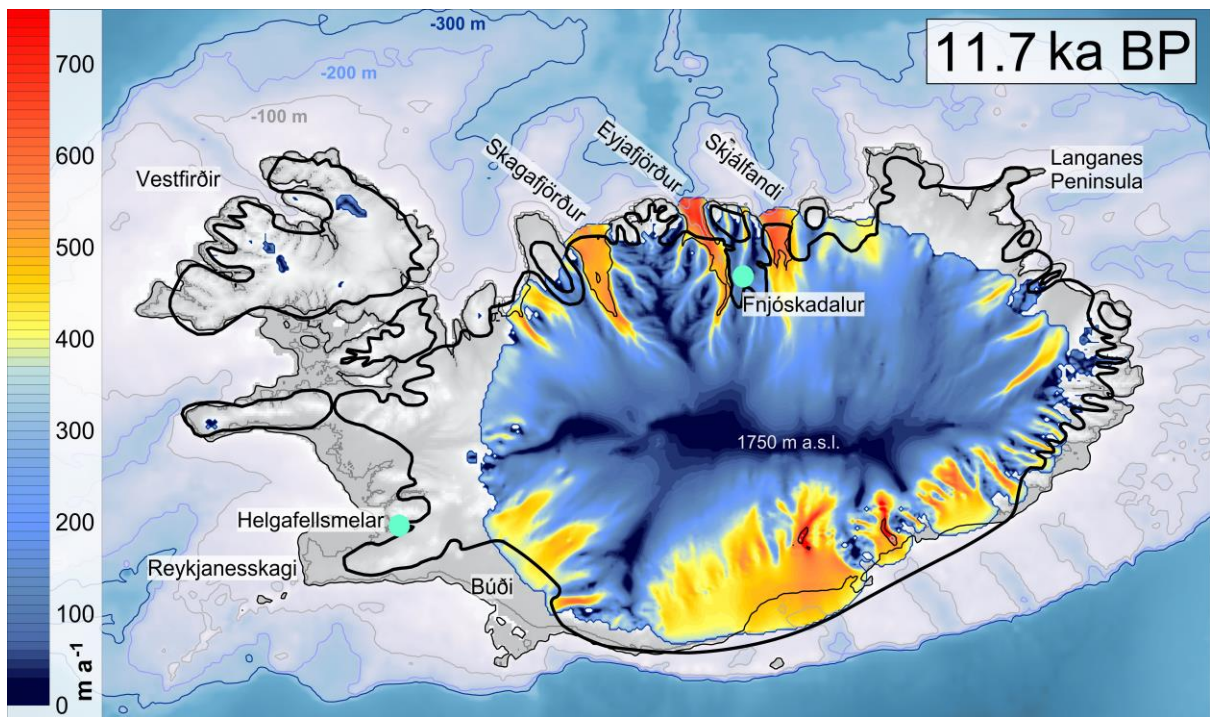
1036

1037

1038   Figure 13
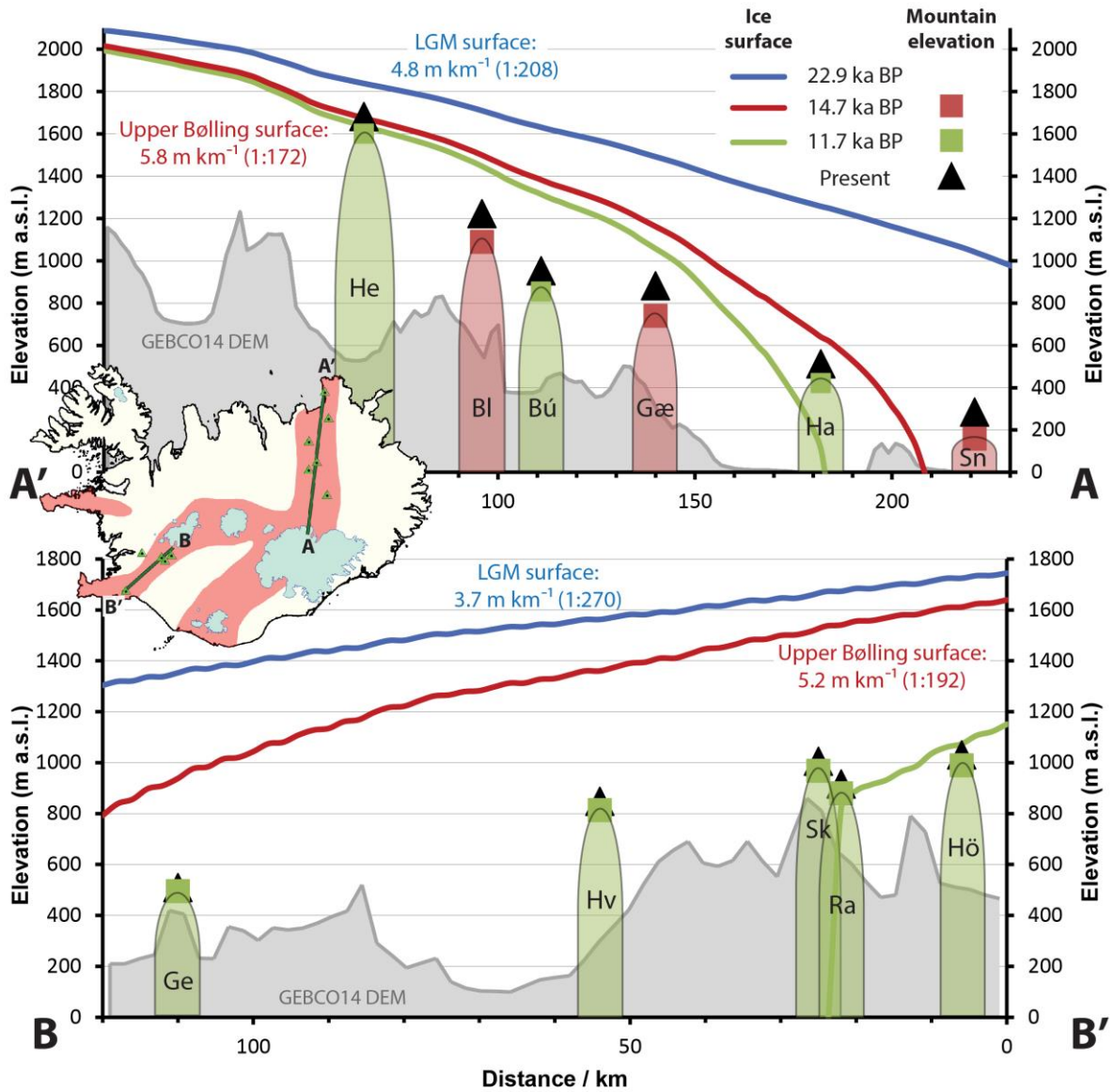
1039

1040

Table captions

1042 Table 1: Reported ^{14}C ages were recalibrated (unless starred) using the program Calib 7.1 (Stuiver
1043 and Reimer, 1993) and the IntCal13/MARINE13 calibration curves (Reimer et al., 2013). A ΔR value of
1044 24±23 was used to account for local effects on the global reservoir correction (Håkansson, 1983).

1045 Table 2: Principal parameters, constants and values used to force the ice-sheet model.

1046 Table 3: Sensitivity of the reference experiment to magnitude changes of model parameters that
1047 control ice flow, calving, sea-level forcing and the basal geothermal heat flux. Variations in the MAAT
1048 climate forcing are shifted prior to 28.5 ka BP to influence the pre-LGM size of the ice sheet. Scaled
1049 variations of G are based upon the present-day distribution (including the neovolcanic zones). Ice
1050 volume, area, thickness values are taken from the maximal ice-sheet timeslice.

1051 Table 4: Principal components of mass loss post LGM.

1052

Table 1

Core/Lab ID	Source	Lat N	Long W	Uncorrected age (^{14}C yr BP)	Median probability age (cal. ka BP)	2σ range (cal. ka BP)	Notes
Jökuldjúp							
AA-12896	Syvitski et al. [1999]; Jennings et al. [2000]	64 17.06	24 12.42	13,105 ± 85	15,068	14,652 – 15,368	*N. labradorica* found in glacial marine unit with dropstones. Within 1 m of the underlying ice contact deposit. Sampled from the core cutter.
MD99-2256	Principato et al. [2005]	64 18.19	24 12.4	12,990 ± 80	14,850	14,337 – 15,174	Mollusc at base of glacimarine sediments
Latra Bank							
96-1227GGC	Syvitski et al. [1999]	65 47.0	26 19.5	36,050 ± 560	40,215	38,970 – 41,369	*Cibicides lobatulus* from possible exposed older (pre LGM) sediments due to glacial erosion
96-1220GGC	Andrews et al. [2000]	65 0.0	27 30.0	18,090 ± 80	21,364	21,045 – 21,660	*N. pachyderma*
JM96-1221GGC		65 7.9	27 32.2	18,240 ± 80	21,579	21,301 – 21,849	
Djúpáll							
JM96-1234GGC	Andrews et al. [2000]	66 35.15	23 58.8	15,720 ± 70	18,564	18,373 – 18,735	Mixed benthics from the base of core.
B997-338PC	Andrews et al. [2002]	66 35.3	23 58.6	19,280 ± 420	22,761	21,809 – 23,759	Sample located within rhythmic laminations above diamict. Material unreported.
				34,600 ± 640	38,599	36,771 – 40,056	Unreported foraminifera within diamict underlying laminated marine deposits
Northern troughs							
97-317PC	Andrews et al. [2000]	66 35.27	18 51.9	12,270 ± 100	13,702	13,454 – 13,947	*N. labradoricum* and *C. teretis*
B997-322PC		66 56.29	19 6.5	42,600 ± 3,050	45,590	41,333 – *	Mixed benthic and planktic forams c. 1 m within massive matrix supported diamicton.
B997-323PC1	Andrews & Helgadóttir [2003]	66 50.78	20 13.64	25,330 ± 640	29,018	27,776 – 30,457	Mixed benthic and planktic forams, c. 2 m within massive matrix supported diamicton.
				13,440 ± 190	15,569	15,021 – 16,166	Mixed benthic and planktic forams, at the base of glacimarine muds above massive matrix supported diamicton (till).
B997-326PC1	Principato et al. [2005]	66 36.35	20 54.82	13,835 ± 215	16,133	15,457 – 16,810	Mixed benthic and planktic foraminifera within fine-grained sediments (marine).
	Andrews & Helgadóttir [2003]			23,570 ± 340	27,385	26,615 – 27,892	Mixed benthic foraminifera at the interface between massive matrix supported diamicton and fine-grained sediments (marine).
HM107-04		67 13.63	19 3.0	12,040 ± 80	13,464	13,292 – 13,675	Foraminifera, total benthic fauna within marine sediments

HM107-05	Eiríksson et al. [2000]	66 54.32 17 54.31	14,100 ± 140	16,506	16,102 – 16,969	Foraminifera, *Neogloboquadrina pachyderma* sinistral
Búdi moraines						
AAR-1241	Geirsdóttir et al. [1997]	Búdafoss	10,290 ± 140	11,340	10,943 – 11,878	*Balanus balanus* within uppermost glaciomarine unit
Lu-2403	Hjartarson and Ingólfsson [1988]	Búdafoss	10,220 ± 90	11,197	10,938 – 11,563	*Balanus balanus* on the surface of diamictite
Reykjanesskagi						
U-2898	Norðdahl [1991]	Varmá, Helgafelssmelar	10,780 ± 110	12,197	11,796 – 12,566	*Balanus balanus* collected in the lowermost part of a gravel pit in a raised terrace
AAR-2803	Jóhannesson et al. [1997]; Norðdahl & Pétursson [2005]	Sandgerði	24,510 ± 200	28,130	27,751 – 28,567	*Hyatella arctica* shell fragments from basal till atop striated (215°) bedrock
AAR-2573 - AAR-2577; Beta-82638		Njarðvíkurheiði	21,890 ± 105	25,777	25,561 – 25,976	Weighted mean age from 6 marine shell samples from stratified silty fine sand resting on glacially striated (9°) bedrock
AAR-1900			28,100 ± 410	31,571	30,954 – 32,640	*Mya truncata samples* within marine, bioturbated diamictite above subglacial tillite and glacially striated (340°) lava flow.
AAR-1901	Eiríksson et al. [1997]	Sudernes	28,750 ± 480	32,288	31,289 – 33,441	
Western Iceland						
S-291	Ashwell [1975]	Grjóteyri	12,800 ± 200	14,504	13,884 – 15,170	Shells within marine drift 15-21 m a.s.l.
AAR-3734	Magnusdóttir & Norðdahl	Stora-Fellsöxl	12,940 ± 80	14,736	14,268 – 15,111	Whalebone 80 m a.s.l., constraining a marine limit of 105 m a.s.l.
Ua-21222	Ingólfsson & Norðdahl [2001]	Stóri-Sandhóll	12,975 ± 105	14,792	14,252 – 15,185	Mollusc 135 m a.s.l., constraining a marine limit of 150 m a.s.l.
Lu-3118	Ingólfsson et al. [1995]	Helgafellsmelar	10,580 ± 90	11,793	11,327 – 12,158	*Balanus balanus* shells in sandy layers within a glacimarine diamicton unit, above subglacial till.
Eastern Iceland						
T-4468	Pétursson 1986	Hvalvik	13,020 ± 90	14,898	14,363 – 15,236	Constraining a marine limit 50-60 m a.s.l.

1054

Table 2

Parameter		Value	Units
g	Gravity	9.81	m s^{-2}
ρ	Density of ice	910	kg m^{-3}
ρ_w	Density of sea water	1028	kg m^{-3}
N	Glen flow-law exponent	3	
A_{weert}	Weertman sliding parameter	7.5×10^{-14}	
m	Sliding-law exponent	$1 - 3$	
SF	Sliding factor	5	
A_s	Sliding-law coefficient	1.8×10^{-5}	m kPa^{-3} a^{-1}
A_0	Deformation enhancement	2.5	
A_c	Calving parameter	24.4	a^{-1}
PDD_{ice}	PDD coefficient for ice	0.008	m °C m^{-1} d^{-1}
PDD_{snow}	PDD coefficient for snow|	0.003	m °C m^{-1} d^{-1}
T	Temperature	-	K
T^*	(pressure melt corrected)	$T - 8.7 \times 10^{-4} (S - z)$	K
$T_{snow\text{-}rain}$	Snow-rain threshold	1.0	°C
R	Gas constant	8.314	J mol^{-1} K^{-1}
k_i	Thermal conductivity	$2115.3 + 7.93 (T-273.15)$	J m^{-1} K^{-1} a^{-1}
C_p	Specific heat capacity	$3.1 \times 10^8 \exp(-0.0057T)$	J kg^{-1} K^{-1} a^{-1}
φ	Internal frictional heating		J m^{-3} a^{-1}
G	Geothermal heat flux	$55 - 308$	mW m^{-2}
D	Flexural rigidity	5.0×10^{20}	N m
δt	Time step	0.03	a
δx_i	Finite difference interval	2×10^3	m
x_{min}		-2183000	Gall stereographic
x_{max}	Domain dimensions	-884000	Gall stereographic
x_{min}		6666000	Gall stereographic
x_{max}		7315000	Gall stereographic

1056

1057

1058   Table 3

Experiment	Parameter	Area (x10⁵ km²)	Δ (%)	Thickness (m)	Δ (%)	Volume (x10⁵ km³)	Δ (%)
Reference		5.615	0	1172	0	6.582	0
Hubbard (2006)		3.290	-41.41	939	-19.88	3.090	-53.06
T -2 °C	Pre-LGM	5.508	-1.91	1164	-0.72	6.410	-2.61
T +2 °C	MAAT	5.589	-0.47	1167	-0.48	6.520	-0.95
A_{weert} x 10⁻¹	Sliding	5.537	-1.39	1236	5.45	6.845	3.99
A_{weert} x 10¹		5.466	-2.66	909	-22.48	4.967	-24.54
1.5G (136-616 mW m⁻²)	Geothermal heat flux	5.615	0.00	1172	0.00	6.582	0.00
0.5*G* (34-154 mW m⁻²)		5.616	0.02	1173	0.04	6.586	0.06
0.25*G* (17-77 mW m⁻²)		5.667	0.92	1187	1.28	6.728	2.21
0.1*G* (7-31 mW m⁻²)		5.577	-0.68	1229	4.87	6.856	4.16
C − 0.1 (+100%)	Calving	6.595	17.46	1166	-0.50	7.692	16.86
C + 0.1 (-100%)		4.362	-22.31	1072	-8.58	4.675	-28.97
SL$_{max}$ -50 m	Relative sea-level	5.777	2.89	1175	0.21	6.787	3.11
SL$_{max}$ +50 m		4.985	-11.23	1127	-3.86	5.617	-14.66

1059

1060   Table 4

Period (ka BP)	Total calving losses (Gt)	%	Total surface melt (Gt)	%	Total volume loss (Gt)
21.80 − 18.00 (to present E coast)	63,601	45.2	77,060	54.8	140,636
16.3 − 14.90 (pinned on coast)	8,686	35.0	16,150	65.0	24,831
14.90 − 14.16 (Bølling warming)	2,173	8.9	22,136	91.1	24,302
14.16 − 10.00 (Late Glacial)	1,230	3.8	31,574	96.2	32,794

1061

References

Andersen, K.K., Azuma, N., Barnola, J.-M., Bigler, M., Biscaye, P., Caillon, N., Chappellaz, J., Clausen, H.B., Dahl-Jensen, D., Fischer, H., Flückiger, J., Fritzsche, D., Fujii, Y., Goto-Azuma, K., Grønvold, K., Gundestrup, N.S., Hansson, M., Huber, C., Hvidberg, C.S., Johnsen, S.J., Jonsell, U., Jouzel, J., Kipfstuhl, S., Landais, A., Leuenberger, M., Lorrain, R., Masson-Delmotte, V., Miller, H., Motoyama, H., Narita, H., Popp, T., Rasmussen, S.O., Raynaud, D., Rothlisberger, R., Ruth, U., Samyn, D., Schwander, J., Shoji, H., Siggard-Andersen, M.-L., Steffensen, J.P., Stocker, T., Sveinbjörnsdóttir, a E., Svensson, A., Takata, M., Tison, J.-L., Thorsteinsson, T., Watanabe, O., Wilhelms, F., White, J.W.C., 2004. High-resolution record of Northern Hemisphere climate extending into the last interglacial period. Nature 431, 147–151. doi:10.1038/nature02805

Andrews, J.T., 2007. Holocene denudation of Iceland as determined from accumulation of sediments on the continental margin. Boreas 36, 240–252.

Andrews, J.T., 2005. Late Quaternary marine sediment studies of the Iceland shelf, Paleoceanography and land/ice sheet/ocean interactions, in: Caseldine, C., Russel, A., Hardardóttir, J., Knudsen, O. (Eds.), Iceland - Modern Processes and Past Environments. Elsevier, London, pp. 5–24.

Andrews, J.T., Cooper, T.A., Jennings, A.E., Stein, A.B., Erlenkeuser, H., 1998. Late Quaternary iceberg-rafted detritus events on the Denmark Strait–Southeast Greenland continental slope (~65°N): related to North Atlantic Heinrich events? Mar. Geol. 149, 211–228. doi:10.1016/S0025-3227(98)00029-2

Andrews, J.T., Geirsdóttir, A., Hardardóttir, J., Principato, S., Grönvold, K., Kristjansdóttir, G.B., Helgadóttir, G., Drexler, J., Sveinbjörnsdóttir, A., 2002a. Distribution, sediment magnetism and geochemistry of the Saksunarvatn (10 180 ± 60 cal. yr BP) tephra in marine, lake, and terrestrial sediments, northwest Iceland. J. Quat. Sci. 17, 731–745. doi:10.1002/jqs.727

Andrews, J.T., Hardardóttir, J., Geirsdóttir, Á., Helgadóttir, G., 2002b. Late Quaternary ice extent and glacial history from the Djúpáll trough, off Vestfirdir peninsula, north-west Iceland: a stacked 36 cal. Ky environmental record. Polar Res. 21, 211–226. doi:10.1111/j.1751-8369.2002.tb00074.x

Andrews, J.T., Hardardóttir, J., Helgadóttir, G., Jennings, A.E., Geirsdóttir, Á., Sveinbjörnsdóttir, Á.E., Schoolfield, S., Kristjánsdóttir, G.B., Smith, L.M., Thors, K., Syvitski, J.P.M., 2000. The N and W Iceland Shelf: insights into Last Glacial Maximum ice extent and deglaciation based on acoustic stratigraphy and basal radiocarbon AMS dates. Quat. Sci. Rev. 19, 619–631.

Andrews, J.T., Helgadóttir, G., 2003. Late Quaternary ice cap extent and deglaciation, Húnaflóaáll, northwest Iceland: evidence from marine cores. Arctic, Antarct. Alp. Res. 35, 218–232. doi:10.1657/1523-0430(2003)035[0218:LQICEA]2.0.CO;2

Andrews, J.T.T., 2008. The role of the Iceland Ice Sheet in the North Atlantic during the late Quaternary: a review and evidence from Denmark Strait. J. Quat. Sci. 23, 3–19. doi:10.1002/jqs

Ashwell, I.Y., 1975. Glacial and Late Glacial Processes in Western Iceland. Geogr. Ann. Ser. A, Phys. Geogr. 57, 225–245.

Auriac, A., Spaans, K.H., Sigmundsson, F., Hooper, A., Schmidt, P., Lund, B., 2013. Iceland rising: Solid Earth response to ice retreat inferred from satellite radar interferometry and visocelastic modeling. J. Geophys. Res. Solid Earth 118, 1331–1344. doi:10.1002/jgrb.50082

Ballantyne, C.K., 2010. Extent and deglacial chronology of the last British-Irish Ice Sheet: implications of exposure dating using cosmogenic isotopes. J. Quat. Sci. 25, 515–534. doi:10.1002/jqs.1310

Bamber, J.L., Griggs, J.A., Hurkmans, R.T.W.L., Dowdeswell, J.A., Gogineni, S.P., Howat, I., Mouginot,

1107   J., Paden, J., Palmer, S., Rignot, E., Steinhage, D., 2013. A new bed elevation dataset for
1108   Greenland. Cryosph. 7, 499–510. doi:10.5194/tc-7-499-2013

1109   Björnsson, H., Jónsson, T., Gylfadóttir, S.S., Ólason, E.O., 2007. Mapping the annual cycle of
1110   temperature in Iceland. Meteorol. Zeitschrift 16, 45–56.

1111   Blankenship, D.D., Bell, R.E., Hodge, S.M., Brozena, J.M., Behrendt, J.C., Finn, C.A., 1993. Active
1112   volcanism beneath the West Antarctic ice sheet and implications for ice-sheet stability. Nature
1113   361, 526–529.

1114   Blatter, H., 1995. Velocity and stress-fields in grounded glaciers - a simple algorithm for including
1115   deviatoric stress gradients. J. Glaciol. 41, 333–344. doi:10.3198/1995JoG41-138-333-344

1116   Boulton, G.S., Jarvis, J., Thors, K., 1988. Dispersal of glacially derived sediment over part of the
1117   continental shelf of south Iceland and the geometry of the resultant sediment bodies. Mar.
1118   Geol. 83, 193–223.

1119   Bourgeois, O., Dauteuil, O., Vliet-Lanoë, B. Van, 2000. Geothermal control on flow patterns in the
1120   Last Glacial Maximum ice sheet of Iceland. Earth Surf. Process. Landforms 25, 59–76.

1121   Brown, C.S., Meier, M.F., Post, A., 1982. Calving speed of Alaskan tidewater glaciers, with application
1122   to Columbia Glacier, US Geological Survey Professional Paper 1258-C.

1123   Brynjólfsson, S., Schomacker, A., Ingólfsson, Ó., Keiding, J.K., 2015. Cosmogenic 36Cl exposure ages
1124   reveal a 9.3 ka BP glacier advance and the Late Weichselian-Early Holocene glacial history of
1125   the Drangajökull region, northwest Iceland. Quat. Sci. Rev. 126, 140–157.
1126   doi:10.1016/j.quascirev.2015.09.001

1127   Caseldine, C., Geirsdóttir, Á., Langdon, P., 2003. Efstadalsvatn – a multi-proxy study of a Holocene
1128   lacustrine sequence from NW Iceland. J. Paleolimnol. 30, 55–73.
1129   doi:10.1023/A:1024781918181

1130   Chandler, D.M., Hubbard, A.L., Hubbard, B.P., Nienow, P.W., 2006. A Monte Carlo error analysis for
1131   basal sliding velocity calculations. J. Geophys. Res. Earth Surf. 111, F04005.
1132   doi:10.1029/2006JF000476

1133   Chauché, N., Hubbard, A., Gascard, J.-C., Box, J.E., Bates, R., Koppes, M., Sole, A., Christoffersen, P.,
1134   Patton, H., 2014. Ice–ocean interaction and calving front morphology at two west Greenland
1135   tidewater outlet glaciers. Cryosph. 8, 1457–1468. doi:10.5194/tc-8-1457-2014

1136   Clark, C.D., 1993. Mega-scale glacial lineations and cross-cutting ice-flow landforms. Earth Surf.
1137   Process. Landforms 18, 1–29.

1138   Clark, C.D., Hughes, A.L.C., Greenwood, S.L., Jordan, C., Sejrup, H.P., 2012. Pattern and timing of
1139   retreat of the last British-Irish Ice Sheet. Quat. Sci. Rev. 44, 112–146.
1140   doi:10.1016/j.quascirev.2010.07.019

1141   Clark, P.U., Dyke, A.S., Shakun, J.D., Carlson, A.E., Clark, J., Wohlfarth, B., Mitrovica, J.X., Hostetler,
1142   S.W., McCabe, a M., 2009. The Last Glacial Maximum. Science 325, 710–714.
1143   doi:10.1126/science.1172873

1144   Corr, H.F.J., Vaughan, D.G., 2008. A recent volcanic eruption beneath the West Antarctic ice sheet.
1145   Nat. Geosci. 1, 122–125. doi:10.1038/ngeo106

1146   Crochet, P., Jóhannesson, T., Jónsson, T., Sigur\dhsson, O., Björnsson, H., Pálsson, F., Barstad, I.,
1147   2007. Estimating the spatial distribution of precipitation in Iceland using a linear model of
1148   orographic precipitation. J. Hydrometeorol. 8, 1285–1306.

1149   Dansgaard, W., White, J.W.C., Johnsen, S.J., 1989. The abrupt termination of the Younger Dryas

1150   climate event. Nature 339, 532–534. doi:10.1038/339532a0

1151   Deschamps, P., Durand, N., Bard, E., Hamelin, B., Camoin, G., Thomas, A.L., Henderson, G.M., Okuno,
1152   J., Yokoyama, Y., 2012. Ice-sheet collapse and sea-level rise at the Bølling warming 14,600 years
1153   ago. Nature 483, 559–564. doi:10.1038/nature10902

1154   Dowdeswell, J.A., Evans, J., Ó Cofaigh, C., 2010. Submarine landforms and shallow acoustic
1155   stratigraphy of a 400 km-long fjord-shelf-slope transect, Kangerlussuaq margin, East Greenland.
1156   Quat. Sci. Rev. 29, 3359–3369. doi:10.1016/j.quascirev.2010.06.006

1157   Dyke, A., 2004. An outline of North American deglaciation with emphasis on central and northern
1158   Canada, in: Ehlers, J., Gibbard, P.L. (Eds.), Quaternary Glaciations - Extent and Chronology Part
1159   2: North America. Elsevier, pp. 371–406.

1160   Egloff, J., Johnson, G.L., 1979. Erosional and depositional structures of the southwest Iceland insular
1161   margin: thirteen geophysical profiles, in: Watkins, J.S., Montadert, L., Dickerson, P.W. (Eds.),
1162   Geological and Geophysical Investigations of Continental Margins, Geological and Geophysical
1163   Investigations of Continental Margins. American Association of Petroleum Geologists, Tulsa,
1164   Oklahoma, pp. 43–63.

1165   Einarsson, T., 1968. Jarðfræði, saga bergs og lands. Mál og Menning, Reykjavík.

1166   Eiríksson, J., Knudsen, K.L., Haflidason, H., Henriksen, P., 2000. Late-glacial and Holocene
1167   palaeoceanography of the North Icelandic shelf. J. Quat. Sci. 15, 23–42. doi:10.1002/(SICI)1099-
1168   1417(200001)15:1<23::AID-JQS476>3.0.CO;2-8

1169   Eiríksson, J., Símonarson, L.A., Knudsen, K.L., Kristensen, P., 1997. Fluctuations of the Weichselian ice
1170   sheet in SW Iceland: a glaciomarine sequence from Sudurnes, Seltjarnarnes. Quat. Sci. Rev. 16,
1171   221–240. doi:10.1016/S0277-3791(96)00052-2

1172   Engelhardt, H., 2004. Ice temperature and high geothermal flux at Siple Dome, West Antarctica,
1173   from borehole measurements. J. Glaciol. 50, 251–256. doi:10.3189/172756504781830105

1174   Fabel, D., Stroeven, A.P., Harbor, J., Kleman, J., Elmore, D., Fink, D., 2002. Landscape preservation
1175   under Fennoscandian ice sheets determined from in situ produced 10Be and 26Al. Earth Planet.
1176   Sci. Lett. 201, 397–406. doi:10.1016/S0012-821X(02)00714-8

1177   Fahnestock, M., Abdalati, W., Joughin, I., Brozena, J., Gogineni, P., 2001. High geothermal heat flow,
1178   basal melt, and the origin of rapid ice flow in central Greenland. Science 294, 2338–2342.

1179   Fisher, A.T., Mankoff, K.D., Tulaczyk, S.M., Tyler, S.W., Foley, N., 2015. High geothermal heat flux
1180   measured below the West Antarctic Ice Sheet. Sci. Adv. 1, e1500093–e1500093.
1181   doi:10.1126/sciadv.1500093

1182   Flóvenz, Ó.G., Sæmundsson, K., 1993. Heat flow and geothermal processes in Iceland.
1183   Tectonophysics 225, 123–138.

1184   Fretwell, P., Pritchard, H.D., Vaughan, D.G., Bamber, J.L., Barrand, N.E., Bell, R., Bianchi, C., Bingham,
1185   R.G., Blankenship, D.D., Casassa, G., Catania, G., Callens, D., Conway, H., Cook, A.J., Corr, H.F.J.,
1186   Damaske, D., Damm, V., Ferraccioli, F., Forsberg, R., Fujita, S., Gim, Y., Gogineni, P., Griggs, J.A.,
1187   Hindmarsh, R.C.A., Holmlund, P., Holt, J.W., Jacobel, R.W., Jenkins, A., Jokat, W., Jordan, T.,
1188   King, E.C., Kohler, J., Krabill, W., Riger-Kusk, M., Langley, K.A., Leitchenkov, G., Leuschen, C.,
1189   Luyendyk, B.P., Matsuoka, K., Mouginot, J., Nitsche, F.O., Nogi, Y., Nost, O.A., Popov, S. V.,
1190   Rignot, E., Rippin, D.M., Rivera, A., Roberts, J., Ross, N., Siegert, M.J., Smith, A.M., Steinhage,
1191   D., Studinger, M., Sun, B., Tinto, B.K., Welch, B.C., Wilson, D., Young, D.A., Xiangbin, C.,
1192   Zirizzotti, A., 2013. Bedmap2: improved ice bed, surface and thickness datasets for Antarctica.
1193   Cryosph. 7, 375–393. doi:10.5194/tc-7-375-2013

1194   Geirsdóttir, Á., 2011. Pliocene and Pleistocene Glaciations of Iceland: A Brief Overview of the Glacial
1195   History, in: Ehlers, Jürgen, Gibbard, P.L., Hughes, P.D. (Eds.), Quaternary Glaciations - Extent
1196   and Chronology. A Closer Look. Elsevier, pp. 199–260.

1197   Geirsdóttir, Á., Andrews, J.T., Ólafsdóttir, S., Helgadóttir, G., Hardardóttir, J., 2002. A 36 ka record of
1198   iceberg rafting and sedimentation from NW Iceland. Following the ice retreat from the shelf to
1199   land. Polar Res. 21, 291–298.

1200   Geirsdóttir, Á., Eiriksson, J., 1994. Sedimentary facies and environmental history of the Late-glacial
1201   glaciomarine Fossvogur sediments in Reykjavík, Iceland. Boreas 23, 164–176.
1202   doi:10.1111/j.1502-3885.1994.tb00597.x

1203   Geirsdóttir, Á., Hardardóttir, J., Eiríksson, J., 1997. The depositional history of the Younger Dryas-
1204   Preboreal Búði moraines in south-central Iceland. Arct. Alp. Res. 29, 13–23.

1205   Geirsdóttir, Á., Hardardóttir, J., Sveinbjörnsdóttir, Á.E., 2000. Glacial extent and catastrophic
1206   meltwater events during the deglaciation of Southern Iceland. Quat. Sci. Rev. 19, 1749–1761.

1207   Geirsdóttir, Á., Jennings, A.E., Lacasse, C., Hardadóttir, J., 1999. Record of jökullhlaup activities in
1208   Iceland during the late Younger Dryas and the Preboreal - evidence from land, near-shore, shelf
1209   and deep-sea sediments. Geol. Soc. Am. Abstr. with Programs 1, 314.

1210   Geirsdóttir, Á., Miller, G.H., Andrews, J.T., 2007. Glaciation, erosion, and landscape evolution of
1211   Iceland. J. Geodyn. 43, 170–186.

1212   Geirsdóttir, Á., Miller, G.H., Axford, Y., Sædís Ólafsdóttir, 2009. Holocene and latest Pleistocene
1213   climate and glacier fluctuations in Iceland. Quat. Sci. Rev. 28, 2107–2118.
1214   doi:10.1016/j.quascirev.2009.03.013

1215   Geyer, A., Bindeman, I., 2011. Glacial influence on caldera-forming eruptions. J. Volcanol. Geotherm.
1216   Res. 202, 127–142. doi:10.1016/j.jvolgeores.2011.02.001

1217   Glen, J., 1955. The creep of polycrystalline ice. Proc. R. Soc. London, Ser. A 228, 519–538.

1218   Golledge, N., Hubbard, A., Bradwell, T., 2010. Influence of seasonality on glacier mass balance, and
1219   implications for palaeoclimate reconstructions. Clim. Dyn. 35, 757–770. doi:10.1007/s00382-
1220   009-0616-6

1221   Golledge, N.R., Hubbard, A., Sugden, D.E., 2008. High-resolution numerical simulation of Younger
1222   Dryas glaciation in Scotland. Quat. Sci. Rev. 27, 888–904. doi:10.1016/j.quascirev.2008.01.019

1223   Greve, R., 2005. Relation of measured basal temperatures and the spatial distribution of the
1224   geothermal heat flux for the Greenland ice sheet. Ann. Glaciol. 42, 424–432.
1225   doi:10.3189/172756405781812510

1226   Greve, R., Hutter, K., 1995. Polythermal three-dimensional modelling of the Greenland ice sheet with
1227   varied geothermal heat flux. Ann. Glaciol. 21, 8–12.

1228   Grönvold, K., Oskarsson, N., Johnsen, S.J., Clausen, H.B., Hammer, C.U., Bond, G., Bard, E., 1995. Ash
1229   layers from Iceland in the Greenland GRIP ice core correlated with oceanic and land sediments.
1230   Earth Planet. Sci. Lett. 135, 149–155.

1231   Gudmundsson, M.T., Sigmundsson, F., Björnsson, H., 1997. Ice-volcano interaction of the 1996 Gjálp
1232   subglacial eruption, Vatnajökull, Iceland. Nature 389, 954–957. doi:10.1038/40122

1233   Håkansson, S., 1983. A reservoir age for the coastal waters of Iceland. Geol. Föreningen i Stock.
1234   Förhandlingar 105, 64–67. doi:10.1080/11035898309455300

1235   Hanna, E., Navarro, F.J., Pattyn, F., Domingues, C.M., Fettweis, X., Ivins, E.R., Nicholls, R.J., Ritz, C.,
1236   Smith, B., Tulaczyk, S., Whitehouse, P.L., Zwally, H.J., 2013. Ice-sheet mass balance and climate

1237   change. Nature 498, 51–9. doi:10.1038/nature12238

1238   Hindmarsh, R.C.A., 2004. A numerical comparison of approximations to the Stokes equations used in
1239   ice sheet and glacier modeling. J. Geophys. Res. Earth Surf. 109, F01012.
1240   doi:10.1029/2003JF000065

1241   Hindmarsh, R.C.A., 1993. Modeling the dynamics of ice sheets. Prog. Phys. Geogr. 17, 391–412.

1242   Hjartarson, Á., Ingólfsson, Ó., 1988. Preboreal glaciation of Southern Iceland. Jökull 38, 1–16.

1243   Hjort, C., Ingólfsson, Ó., Norðdahl, H., 1985. Late Quaternary geology and glacial history of
1244   Hornstrandir, Northwest Iceland: a reconnaissance study. Jökull 38, 9–29.

1245   Hoff, U., Rasmussen, T.L., Stein, R., Ezat, M.M., Fahl, K., 2016. Sea ice and millennial-scale climate
1246   variability in the Nordic seas 90 kyr ago to present. Nat. Commun. 7:12247.
1247   doi:10.1038/ncomms12247

1248   Hoppe, G., 1968. Grimsey and the maximum extent of the last glaciation of Iceland. Geogr. Ann. Ser.
1249   A, Phys. Geogr. 50, 16–24.

1250   Howat, I.M., Joughin, I., Scambos, T.A., 2007. Rapid changes in ice discharge from Greenland outlet
1251   glaciers. Science 315, 1559–61. doi:10.1126/science.1138478

1252   Hubbard, A., 2006. The validation and sensitivity of a model of the Icelandic ice sheet. Quat. Sci. Rev.
1253   25, 2297–2313. doi:10.1016/j.quascirev.2006.04.005

1254   Hubbard, A., 2000. The verification and significance of three approaches to longitudinal stresses in
1255   high-resolution models of glacier flow. Geogr. Ann. Ser. A, Phys. Geogr. 82, 471–487.
1256   doi:10.1111/j.0435-3676.2000.00135.x

1257   Hubbard, A., 1999. High-resolution modeling of the advance of the Younger Dryas ice sheet and its
1258   climate in Scotland. Quat. Res. 52, 27–43. doi:10.1006/qres.1999.2055

1259   Hubbard, A., Blatter, H., Nienow, P., Mair, D., Hubbard, B., 1998. Comparison of a three-dimensional
1260   model for glacier flow with field data from Haut Glacier d'Arolla, Switzerland. J. Glaciol. 44,
1261   368–378. doi:10.3198/1998JoG44-147-368-378

1262   Hubbard, A., Bradwell, T., Golledge, N., Hall, A., Patton, H., Sugden, D., Cooper, R., Stoker, M., 2009.
1263   Dynamic cycles, ice streams and their impact on the extent, chronology and deglaciation of the
1264   British–Irish ice sheet. Quat. Sci. Rev. 28, 758–776. doi:10.1016/j.quascirev.2008.12.026

1265   Hubbard, A., Hein, A.S., Kaplan Michael, R., Hulton, N.R.J., Glasser, N.F., 2005. A modelling
1266   reconstruction of the last glacial maximum ice sheet and its deglaciation in the vicinity of the
1267   Northern Patagonian Icefield, South America. Geogr. Ann. Ser. A, Phys. Geogr. 87, 375–391.
1268   doi:10.1111/j.0435-3676.2005.00264.x

1269   Hubbard, A., Sugden, D., Dugmore, A., Norddahl, H., Pétursson, H.G., 2006. A modelling insight into
1270   the Icelandic Last Glacial Maximum ice sheet. Quat. Sci. Rev. 25, 2283–2296.
1271   doi:10.1016/j.quascirev.2006.04.001

1272   Hubbard, B.P., Hubbard, A., Mader, H.M., Tison, J.-L., Grust, K., Nienow, P.W., 2003. Spatial
1273   variability in the water content and rheology of temperate glaciers: Glacier de Tsanfleuron,
1274   Switzerland. Ann. Glaciol. 37, 1–6. doi:10.3189/172756403781815474

1275   Hughes, A.L.C., Gyllencreutz, R., Lohne, Ø.S., Mangerud, J., Svendsen, J.I., 2016. The last Eurasian ice
1276   sheets – a chronological database and time-slice reconstruction, DATED-1. Boreas 45, 1–45.
1277   doi:10.1111/bor.12142

1278   Ingólfsson, Ó., 1991. A review of the Late Weischelian and early Holocene glacial and environmental
1279   history of Iceland, in: Caseldine, C., Maizels, J.K. (Eds.), Environmental Change in Iceland: Past

1280   and Present. Kluwer Academic Publishers, Netherlands, pp. 13–29.

1281   Ingólfsson, Ó., Björck, S., Haflidason, H., Rundgren, M., 1997. Glacial and climatic events in iceland
1282   reflecting regional north atlantic climatic shifts during the Pleistocene-Holocene transition.
1283   Quat. Sci. Rev. 16, 1135–1144. doi:10.1016/S0277-3791(97)00007-3

1284   Ingólfsson, Ó., Norðdahl, H., 2001. High relative sea level during the Bølling Interstadial in western
1285   Iceland: a reflection of ice-sheet collapse and extremely rapid glacial unloading. Arctic, Antarct.
1286   Alp. Res. 33, 231–243.

1287   Ingólfsson, Ó., Norðdahl, H., 1994. A review of the environmental history of Iceland, 13,000-9000 yr
1288   BP. J. Quat. Sci. 9, 147–150.

1289   Ingólfsson, Ó., Norðdahl, H., Haflidason, H., 1995. Rapid isostatic rebound in southwestern Iceland at
1290   the end of the last glaciation. Boreas 24, 245–259. doi:10.1111/j.1502-3885.1995.tb00777.x

1291   Ingólfsson, Ó., Norðdahl, H., Schomacker, A., 2010. Deglaciation and Holocene Glacial History of
1292   Iceland, in: The Mýrdalsjökull Ice Cap, Iceland. Glacial Processes, Sediments and Landforms on
1293   an Active Volcano, Developments in Quaternary Sciences. Elsevier, pp. 51–68.
1294   doi:10.1016/S1571-0866(09)01304-9

1295   Jakobsson, S.P., Jónsson, J., Shido, F., 1978. Petrology of the western Reykjanes Peninsula, Iceland. J.
1296   Petrol. 19, 669–705.

1297   Jennings, A., Syvitski, J.P.M., Gerson, L., 2000. Chronology and paleoenvironments during the late
1298   Weichselian deglaciation of the southwest Iceland shelf. Boreas 29, 163–183.

1299   Jull, M., McKenzie, D., 1996. The effect of deglaciation on mantle melting beneath Iceland. J.
1300   Geophys. Res. Solid Earth 101, 21815–21828.

1301   Keith, D.B., Jones, E.W., 1935. Grímsey, North Iceland. Geogr. Journal1 86, 143–152.

1302   King, E.C., Hindmarsh, R.C.A., Stokes, C.R., 2009. Formation of mega-scale glacial lineations observed
1303   beneath a West Antarctic ice stream. Nat. Geosci. 2, 585–588.

1304   Koenigk, T., Mikolajewicz, U., Jungclaus, J.H., Kroll, A., 2009. Sea ice in the Barents Sea: seasonal to
1305   interannual variability and climate feedbacks in a global coupled model. Clim. Dyn. 32, 1119–
1306   1138. doi:10.1007/s00382-008-0450-2

1307   Kukkonen, I.T., 1989. Terrestrial heat flow and radiogenic heat production in Finland, the central
1308   Baltic Shield. Tectonophysics 164, 219–230. doi:10.1016/0040-1951(89)90015-2

1309   Lambeck, K., Rouby, H., Purcell, A., Sun, Y., Sambridge, M., 2014. Sea level and global ice volumes
1310   from the Last Glacial Maximum to the Holocene. Proc. Natl. Acad. Sci. U. S. A. 111, 15296–303.
1311   doi:10.1073/pnas.1411762111

1312   Larsen, D.J., Miller, G.H., Geirsdóttir, Á., Ólafsdóttir, S., 2012. Non-linear Holocene climate evolution
1313   in the North Atlantic: a high-resolution, multi-proxy record of glacier activity and
1314   environmental change from Hvítárvatn, central Iceland. Quat. Sci. Rev. 39, 14–25.
1315   doi:10.1016/j.quascirev.2012.02.006

1316   Laumann, T., Reeh, N., 1993. Sensitivity to climate-change of the mass-balance of glaciers in
1317   southern Norway. J. Glaciol. 39, 656–665. doi:10.3198/1993JoG39-133-656-665

1318   Licciardi, J.M., Kurz, M.D., Curtice, J.M., 2007. Glacial and volcanic history of Icelandic table
1319   mountains from cosmogenic 3He exposure ages. Quat. Sci. Rev. 26, 1529–1546.
1320   doi:10.1016/j.quascirev.2007.02.016

1321   Lubimova, E.., Karus, E.., Firsov, F.., Starikova, G.., Vlasov, V.., Lyusova, L.., Koperbakh, E.., 1972.
1322   Terrestrial heat flow on Pre-Cambrian shields in the USSR. Geothermics 1, 81–89.

1323   doi:10.1016/0375-6505(72)90017-X

1324 MacAyeal, D.R., 1993. Binge/purge oscillations of the Laurentide Ice Sheet as a cause of the North
1325   Atlantic's Heinrich Events. Paleoceanography 8, 775–784.

1326 Maclennan, J., Jull, M., McKenzie, D., Slater, L., Grönvold, K., 2002. The link between volcanism and
1327   deglaciation in Iceland. Geochemistry, Geophys. Geosystems 3, 1–25.
1328   doi:10.1029/2001GC000282

1329 Mangerud, J., Gulliksen, S., Larsen, E., 2010. 14C-dated fluctuations of the western flank of the
1330   Scandinavian Ice Sheet 45-25 kyr BP compared with Bølling-Younger Dryas fluctuations and
1331   Dansgaard-Oeschger events in Greenland. Boreas 39, 328–342. doi:10.1111/j.1502-
1332   3885.2009.00127.x

1333 Mangerud, J., Gulliksen, S., Larsen, E., Longva, O., Miller, G.H., Sejrup, H.-P., Sønstegaard, E., 1981. A
1334   Middle Weichselain ice-free period in Western Norway: the Ålesund Interstadial. Boreas 10,
1335   447–462. doi:10.1111/j.1502-3885.1981.tb00508.x

1336 Marshall, S.J., Björnsson, H., Flowers, G.E., Clarke, G.K.C., 2005. Simulation of Vatnajökull ice cap
1337   dynamics. J. Geophys. Res. Earth Surf. 110, F03009. doi:10.1029/2004JF000262

1338 Maule, C.F., Purucker, M.E., Olsen, N., Mosegaard, K., 2005. Heat flux anomalies in Antarctica
1339   revealed by satellite magnetic data. Science 309, 464–467. doi:10.1126/science.1106888

1340 Näslund, J.-O., Jansson, P., Fastook, J.L., Johnson, J., Andersson, L., 2005. Detailed spatially
1341   distributed geothermal heat-flow data for modeling of basal temperatures and meltwater
1342   production beneath the Fennoscandian ice sheet. Ann. Glaciol. 40, 95–101.
1343   doi:10.3189/172756405781813582

1344 Nick, F.M., Luckman, A., Vieli, A., van der Veen, C.J., van As, D., van de Wal, R.S.W., Pattyn, F.,
1345   Hubbard, A.L., Floricioiu, D., 2012. The response of Petermann Glacier, Greenland, to large
1346   calving events, and its future stability in the context of atmospheric and oceanic warming. J.
1347   Glaciol. 58, 229–239. doi:10.3189/2012JoG11J242

1348 Nielsen, T., Rasmussen, T.L., Ceramicola, S., Kuijpers, A., 2007. Quaternary sedimentation, margin
1349   architecture and ocean circulation variability around the Faroe Islands, North Atlantic. Quat.
1350   Sci. Rev. 26, 1016–1036. doi:10.1016/j.quascirev.2006.12.005

1351 Norðdahl, H., 1991. A review of the glaciation maximum concept and the deglacation of Eyjafjördur,
1352   North Iceland, in: Maizels, J.K., Caseldine, C. (Eds.), Environmental Change in Iceland: Past and
1353   Present. Kluwer Academic Publishers, Netherlands, pp. 31–47.

1354 Norðdahl, H., 1983. Late Quaternary stratigraphy of Fnjóskadalur, central North Iceland: a study of
1355   sediments, ice-lake strandlines, glacial isostasy and ice-free areas. Lundqua Thesis 12, Lundqua
1356   thesis. Lund University.

1357 Norðdahl, H., Einarsson, T., 2001. Concurrent changes of relative sea-level and glacier extent at the
1358   Weichselian-Holocene boundary in Berufjörður, Eastern Iceland. Quat. Sci. Rev. 20, 1607–1622.

1359 Norðdahl, H., Haflidason, H., 1992. The Skógar Tephra, a Younger Dryas marker in North Iceland.
1360   Boreas 21, 23–41.

1361 Norðdahl, H., Hjort, C., 1995. Lateglacial raised beaches and glacier recession in the Thistilfjörður-
1362   Bakkaflói area, northeast Iceland. Jökull 43, 32–44.

1363 Norðdahl, H., Ingólfsson, Ó., 2015. Collapse of the Icelandic ice sheet controlled by sea-level rise?
1364   Arktos 1, 1–13. doi:10.1007/s41063-015-0020-x

1365 Norðdahl, H., Ingólfsson, Ó., Pétursson, H.G., Hallsdóttir, M., 2008. Late Weichselian and Holocene

1366   environmental history of Iceland. Jökull 58, 343–364.

1367   Norðdahl, H., Pétursson, G.P., 2005. Relative sea level changes in Iceland: new aspect of the
1368   Weichselian deglaciation of Iceland, in: Caseldine, C., Russel, A., Hardardóttir, J., Knudsen, O.
1369   (Eds.), Iceland - Modern Processes and Past Environments. Elsevier, Amsterdam, pp. 25–78.

1370   Ó Cofaigh, C., 1996. Tunnel valley genesis. Prog. Phys. Geogr. 20, 1–19.
1371   doi:10.1177/030913339602000101

1372   Ó Cofaigh, C., Pudsey, C.J., Dowdeswell, J.A., Morris, P., 2002. Evolution of subglacial bedforms along
1373   a paleo-ice stream, Antarctic Peninsula continental shelf. Geophys. Res. Lett. 29, 1199.

1374   Óladóttir, B.A., Larsen, G., Sigmarsson, O., 2011. Holocene volcanic activity at Grímsvötn,
1375   Bárdarbunga and Kverkfjöll subglacial centres beneath Vatnajökull, Iceland. Bull. Volcanol. 73,
1376   1187–1208. doi:10.1007/s00445-011-0461-4

1377   Ólafsdóttir, T., 1975. Jökulgardur á sjávarbotniit af Breidafirdi (English summary: A moraine ridge on
1378   the Iceland shelf, west of Breidafjördur). Náttúrufrædingurinn 45, 247–271.

1379   Ottesen, D., Dowdeswell, J.A., Rise, L., Rokoengen, K., Henriksen, S., 2002. Large-scale morphological
1380   evidence for past ice-stream flow on the mid-Norwegian continental margin. Geol. Soc.
1381   London, Spec. Publ. 203, 245–258.

1382   Papa, B.D., Mysak, L.A., Wang, Z., 2005. Intermittent ice sheet discharge events in northeastern
1383   North America during the last glacial period. Clim. Dyn. 26, 201–216. doi:10.1007/s00382-005-
1384   0078-4

1385   Patton, H., Andreassen, K., Bjarnadóttir, L.R., Dowdeswell, J.A., Winsborrow, M.C.M., Noormets, R.,
1386   Polyak, L., Auriac, A., Hubbard, A., 2015. Geophysical constraints on the dynamics and retreat
1387   of the Barents Sea Ice Sheet as a palaeo-benchmark for models of marine ice-sheet
1388   deglaciation. Rev. Geophys. 53, 1051–1098. doi:10.1002/2015RG000495

1389   Patton, H., Hubbard, A., Andreassen, K., Winsborrow, M., Stroeven, A.P., 2016. The build-up,
1390   configuration, and dynamical sensitivity of the Eurasian ice-sheet complex to Late Weichselian
1391   climatic and oceanic forcing. Quat. Sci. Rev. 153, 97–121. doi:10.1016/j.quascirev.2016.10.009

1392   Patton, H., Hubbard, A., Glasser, N.F., Bradwell, T., Golledge, N.R., 2013. The last Welsh Ice Cap: Part
1393   1 - Modelling its evolution, sensitivity and associated climate. Boreas 42, 471–490.
1394   doi:10.1111/j.1502-3885.2012.00300.x

1395   Pattyn, F., Perichon, L., Aschwanden, A., Breuer, B., de Smedt, B., Gagliardini, O., Gudmundsson,
1396   G.H., Hindmarsh, R.C.A., Hubbard, A., Johnson, J. V, Kleiner, T., Konovalov, Y., Martin, C., Payne,
1397   A.J., Pollard, D., Price, S., Rückamp, M., Saito, F., Souček, O., Sugiyama, S., Zwinger, T., 2008.
1398   Benchmark experiments for higher-order and full-Stokes ice sheet models (ISMIP–HOM).
1399   Cryosph. 2, 95–108. doi:10.5194/tc-2-95-2008

1400   Peltier, W.R., Fairbanks, R.G., 2006. Global glacial ice volume and Last Glacial Maximum duration
1401   from an extended Barbados sea level record. Quat. Sci. Rev. 25, 3322–3337.
1402   doi:10.1016/j.quascirev.2006.04.010

1403   Pétursson, H.G., 1991. The Weichselian glacial history of West Melrakkaslétta, Northeastern Iceland,
1404   in: Maizels, J.M., Caseldine, C. (Eds.), Environmental Change in Iceland: Past and Present.
1405   Kluwer Academic Publishers, Dordrecht, pp. 49–65.

1406   Pétursson, H.G., Norðdahl, H., Ingólfsson, Ó., 2015. Late Weichselian history of relative sea level
1407   changes in Iceland during a collapse and subsequent retreat of marine based ice sheet. Cuad.
1408   Investig. Geográfica 41, 261. doi:10.18172/cig.2741

1409   Pollard, D., DeConto, R.M., 2007. A coupled ice-sheet/ice-shelf/sediment model applied to a marine-

1410   margin flowline: forced and unforced variations., in: Hambrey, M.J., Christoffersen, P., Glasser,
1411   N.F., Hubbard, B. (Eds.), Glacial Sedimentary Processes and Products. Blackwell Publishing Ltd,
1412   Oxford.

1413   Principato, S.M., Geirsdóttir, Á., Jóhannsdóttir, G.E., Andrews, J.T., 2006. Late Quaternary glacial and
1414   deglacial history of eastern Vestfirdir, Iceland using cosmogenic isotope (36Cl) exposure ages
1415   and marine cores. J. Quat. Sci. 21, 271–285. doi:10.1002/jqs.978

1416   Principato, S.M., Jennings, A.E., Kristjansdottir, G.B., Andrews, J.T., 2005. Glacial-Marine or Subglacial
1417   Origin of Diamicton Units from the Southwest and North Iceland Shelf: Implications for the
1418   Glacial History of Iceland. J. Sediment. Res. 75, 968–983. doi:10.2110/jsr.2005.073

1419   Principato, S.M., Johnson, J.S., 2009. Using a GIS to Quantify Patterns of Glacial Erosion on
1420   Northwest Iceland: Implications for Independent Ice Sheets. Arctic, Antarct. Alp. Res. 41, 128–
1421   137. doi:10.1657/1523-0430-41.1.128

1422   Principato, S.M., Moyer, A.N., Hampsch, A.G., Ipsen, H.A., 2016. Using GIS and streamlined
1423   landforms to interpret palaeo-ice flow in northern Iceland. Boreas n/a-n/a.
1424   doi:10.1111/bor.12164

1425   Quillmann, U., Andrews, J.T., Jennings, A.E., 2009. Radiocarbon Date List XI : Radiocardon dates from
1426   Marine Sediment Cores of the Iceland, Greenland and the Northeast Canada Arctic Shelves and
1427   Nares Strait. Instaar/OP Occasional.

1428   Rasmussen, S.O., Bigler, M., Blockley, S.P., Blunier, T., Buchardt, S.L., Clausen, H.B., Cvijanovic, I.,
1429   Dahl-Jensen, D., Johnsen, S.J., Fischer, H., Gkinis, V., Guillevic, M., Hoek, W.Z., Lowe, J.J., Pedro,
1430   J.B., Popp, T., Seierstad, I.K., Steffensen, J.P., Svensson, A.M., Vallelonga, P., Vinther, B.M.,
1431   Walker, M.J.C., Wheatley, J.J., Winstrup, M., 2014. A stratigraphic framework for abrupt
1432   climatic changes during the Last Glacial period based on three synchronized Greenland ice-core
1433   records: Refining and extending the INTIMATE event stratigraphy. Quat. Sci. Rev. 106, 14–28.
1434   doi:10.1016/j.quascirev.2014.09.007

1435   Reimer, P., Bard, E., Bayliss, A., Beck, J.W., Blackwell, P.G., Ramsey, C.B., Buck, C.E., Cheng, H.,
1436   Edwards, R.L., Friedrich, M., Grootes, P.M., Guilderson, T.P., Haflidason, H., Hajdas, I., Hatté, C.,
1437   Heaton, T.J., Hoffmann, D.L., Hogg, A.G., Hughen, K.A., Kaiser, K.F., Kromer, B., Manning, S.W.,
1438   Niu, M., Reimer, R.W., Richards, D.A., Scott, E.M., Southon, J.R., Staff, R.A., Turney, C.S.M.,
1439   Plicht, J. van der, 2013. IntCal13 and Marine13 Radiocarbon Age Calibration Curves 0–50,000
1440   Years cal BP. Radiocarbon 55, 1869–1887. doi:10.2458/azu_js_rc.55.16947

1441   Rignot, E., Kanagaratnam, P., 2006. Changes in the velocity structure of the Greenland ice sheet.
1442   Science 311, 986–990.

1443   Rignot, E., Koppes, M., Velicogna, I., 2010. Rapid submarine melting of the calving faces of West
1444   Greenland glaciers. Nat. Geosci. 3, 187–191. doi:10.1038/ngeo765

1445   Roberts, D.H., Long, A.J., Schnabel, C., Freeman, S., Simpson, M.J.R., 2008. The deglacial history of
1446   southeast sector of the Greenland Ice Sheet during the Last Glacial Maximum. Quat. Sci. Rev.
1447   27, 1505–1516. doi:10.1016/j.quascirev.2008.04.008

1448   Rogozhina, I., Hagedoorn, J.M., Martinec, Z., Fleming, K., Soucek, O., Greve, R., Thomas, M., 2012.
1449   Effects of uncertainties in the geothermal heat flux distribution on the Greenland Ice Sheet: An
1450   assessment of existing heat flow models. J. Geophys. Res. 117, F02025.

1451   Rogozhina, I., Petrunin, A.G., Vaughan, A.P.M., Steinberger, B., Johnson, J. V., Kaban, M.K., Calov, R.,
1452   Rickers, F., Thomas, M., Koulakov, I., 2016. Melting at the base of the Greenland ice sheet
1453   explained by Iceland hotspot history. Nat. Geosci. 9, 366–369. doi:10.1038/ngeo2689

1454   Rolandone, F., Mareschal, J.-C., Jaupart, C., 2003. Temperatures at the base of the Laurentide Ice

1455   Sheet inferred from borehole temperature data. Geophys. Res. Lett. 30.
1456   doi:10.1029/2003GL018046

1457 Rott, H., Rack, W., Skvarca, P., De Angelis, H., 2002. Northern Larsen Ice Shelf, Antarctica: further
1458   retreat after collapse. Ann. Glaciol. 34, 277–282.

1459 Rundgren, M., Ingólfsson, Ó., 1999. Plant survival in Iceland during periods of glaciation? J. Biogeogr.
1460   26, 387–396. doi:10.1046/j.1365-2699.1999.00296.x

1461 Rundgren, M., Ingólfsson, Ó., Björck, S., Jiang, H., Haflidason, H., 1997. Dynamic sea-level change
1462   during the last deglaciation of northern Iceland. Boreas 26, 201–215. doi:10.1111/j.1502-
1463   3885.1997.tb00852.x

1464 Shepherd, A., Ivins, E.R., A, G., Barletta, V.R., Bentley, M.J., Bettadpur, S., Briggs, K.H., Bromwich,
1465   D.H., Forsberg, R., Galin, N., Horwath, M., Jacobs, S., Joughin, I., King, M.A., Lenaerts, J.T.M., Li,
1466   J., Ligtenberg, S.R.M., Luckman, A., Luthcke, S.B., McMillan, M., Meister, R., Milne, G.,
1467   Mouginot, J., Muir, A., Nicolas, J.P., Paden, J., Payne, A.J., Pritchard, H., Rignot, E., Rott, H.,
1468   Sørensen, L.S., Scambos, T.A., Scheuchl, B., Schrama, E.J.O., Smith, B., Sundal, A. V, van
1469   Angelen, J.H., van de Berg, W.J., van den Broeke, M.R., Vaughan, D.G., Velicogna, I., Wahr, J.,
1470   Whitehouse, P.L., Wingham, D.J., Yi, D., Young, D., Zwally, H.J., 2012. A reconciled estimate of
1471   ice-sheet mass balance. Science 338, 1183–9. doi:10.1126/science.1228102

1472 Siegert, M.J., Dowdeswell, J.A., 1996. Topographic control on the dynamics of the Svalbard-Barents
1473   Sea ice sheet. Glob. Planet. Change 12, 27–39. doi:10.1016/0921-8181(95)00010-0

1474 Sigmundsson, F., 1991. Post-glacial rebound and asthenosphere viscosity in Iceland. Geophys. Res.
1475   Lett. 18, 1131–1134. doi:10.1029/91GL01342

1476 Sigvaldason, G.E., Annertz, K., Nilsson, M., 1992. Effect of glacier loading/deloading on volcanism:
1477   postglacial volcanic production rate of the Dyngjufjöll area, central Iceland. Bull. Volcanol. 54,
1478   385–392.

1479 Sinton, J., Grönvold, K., Saemundsson, K., 2005. Postglacial eruptive history of the Western Volcanic
1480   Zone, Iceland. Geochemistry Geophys. Geosystems 6, Q12009.

1481 Slater, L., Jull, M., McKenzie, D., Gronvöld, K., 1998. Deglaciation effects on mantle melting under
1482   Iceland: results from the northern volcanic zone. Earth Planet. Sci. … 164, 151–164.

1483 Smellie, J.L., 2000. Subglacial eruptions, in: Sigurdsson, H. (Ed.), Encyclopedia of Volcanoes.
1484   Academic Press, San Diego, pp. 403–418.

1485 Spagnolo, M., Clark, C.D., 2009. A geomorphological overview of glacial landforms on the Icelandic
1486   continental shelf. J. Maps 5, 37–52. doi:10.4113/jom.2009.1049

1487 Stokes, C.R., Clark, C.D., 2002. Are long subglacial bedforms indicative of fast ice flow? Boreas 31,
1488   239–249. doi:10.1111/j.1502-3885.2002.tb01070.x

1489 Stokes, C.R., Clark, C.D., 2001. Palaeo-ice streams. Quat. Sci. Rev. 20, 1437–1457.

1490 Stokes, C.R., Margold, M., Clark, C.D., Tarasov, L., 2016. Ice stream activity scaled to ice sheet volume
1491   during Laurentide Ice Sheet deglaciation. Nature 530, 322–326. doi:10.1038/nature16947

1492 Stötter, J., Wastl, M., Caseldine, C., Häberle, T., 1999. Holocene palaeoclimatic reconstruction in
1493   northern Iceland: approaches and results. Quat. Sci. Rev. 18, 457–474. doi:10.1016/S0277-
1494   3791(98)00029-8

1495 Stuiver, M., Reimer, P., 1993. Extended 14C Data Base and Revised Calib 3.0 14C Age Calibration
1496   Program. Radiocarbon 35, 215–230.

1497 Syvitski, J.P., Burrell, D.C., Skei, J.M., 1987. Fjords: Processes and Products. Springer Verlag, New

1498   York.

1499   Syvitski, J.P., Jennings, A.E., Andrews, J.T., 1999. High-resolution seismic evidence for multiple
1500   glaciation across the southwest Iceland Shelf. Arctic, Antarct. Alp. Res. 31, 50–57.

1501   Tarasov, L., Peltier, W.R., 2003. Greenland glacial history, borehole constraints, and Eemian extent. J.
1502   Geophys. Res. 108, 2143. doi:10.1029/2001JB001731

1503   Thomas, E.R., Mulvaney, R., Wolff, E.W., 2008. A change in seasonality in Greenland during a
1504   Dansgaard–Oeschger warming. Ann. Glaciol. 48, 19–24. doi:10.3189/172756408784700590

1505   Thordarson, T., Larsen, G., 2007. Volcanism in Iceland in historical time: Volcano types, eruption
1506   styles and eruptive history. J. Geodyn. 43, 118–152. doi:10.1016/j.jog.2006.09.005

1507   Van Vliet-Lanoë, B., Gudmundsson, Å., Guillou, H., Duncan, R. a., Genty, D., Ghaleb, B., Gouy, S.,
1508   Récourt, P., Scaillet, S., 2007. Limited glaciation and very early deglaciation in central Iceland.
1509   Comptes Rendus Geosci. 339, 1–12. doi:10.1016/j.crte.2006.12.001

1510   Vasskog, K., Langebroek, P.M., Andrews, J.T., Nilsen, J.E.Ø., Nesje, A., 2015. The Greenland Ice Sheet
1511   during the last glacial cycle: Current ice loss and contribution to sea-level rise from a
1512   palaeoclimatic perspective. Earth-Science Rev. 150, 45–67. doi:10.1016/j.earscirev.2015.07.006

1513   Vilmundardóttir, E., Larsen, G., 1986. Productivity pattern of the Veidivötn fissure swarm, Southern
1514   Iceland, in post-glacial times. Preliminary results. 17e Nord. Geol. Helsinki.

1515   Vogel, S.W., Tulaczyk, S., 2006. Ice-dynamical constraints on the existence and impact of subglacial
1516   volcanism on West Antarctic ice sheet stability. Geophys. Res. Lett. 33, L23502.
1517   doi:10.1029/2006GL027345

1518   Walker, G.P.L., 1965. Some aspects of Quaternary volcanism in Iceland. Trans. Leicester Lit. Philos.
1519   Soc. 59, 25–40.

1520   Weertman, J., 1964. The theory of glacier sliding. J. Glaciol. 5, 287–303.

1521   Winberry, J.P., Anandakrishnan, S., 2004. Crustal structure of the West Antarctic rift system and
1522   Marie Byrd Land hotspot. Geology 32, 977–980.

1523   Winsborrow, M.C.M., Andreassen, K., Corner, G.D., Laberg, J.S., 2010. Deglaciation of a marine-
1524   based ice sheet: Late Weichselian palaeo-ice dynamics and retreat in the southern Barents Sea
1525   reconstructed from onshore and offshore glacial geomorphology. Quat. Sci. Rev. 29, 424–442.
1526   doi:10.1016/j.quascirev.2009.10.001

1527